JOURNAL OF GEOPHYSICAL RESEARCH, VOL. 112, D09310, doi:10.1029/2006JD007786, 2007

Aircraft observations of aerosol composition and ageing in New England and Mid-Atlantic States during the summer 2002 New England Air Quality Study field campaign

Lawrence I. Kleinman,[1] Peter H. Daum,[1] Yin-Nan Lee,[1] Gunnar I. Senum,[1] Stephen R. Springston,[1] Jian Wang,[1] Carl Berkowitz,[2] John Hubbe,[2] Rahul A. Zaveri,[2] Fred J. Brechtel,[3] John Jayne,[4] Timothy B. Onasch,[4] and Douglas Worsnop[4]

Received 12 July 2006; revised 22 November 2006; accepted 24 January 2007; published 11 May 2007.

[1] Aerosol chemical composition, size distribution, and optical properties were measured during 17 aircraft flights in New England and Middle Atlantic States as part of the summer 2002 New England Air Quality Study field campaign. An Aerodyne aerosol mass spectrometer (AMS) was operated with a measurement cycle of 30 s, about an order of magnitude faster than used for ground-based measurements. Noise levels within a single measurement period were sub μg m^{-3}. Volume data derived from the AMS were compared with volume measurements from a Passive Cavity Aerosol Spectrometer (PCASP) optical particle detector and a Twin Scanning Electrical Mobility Spectrometer (TSEMS); calculated light scattering was compared with measured values from an integrating nephelometer. The median ratio for AMS/TSEMS volume was 1.25 (1.33 with an estimated refractory component); the median ratio for AMS/nephelometer scattering was 1.18. A dependence of the AMS collection efficiency on aerosol acidity was quantified by a comparison between AMS and PCASP volumes in two high sulfate plumes. For the entire field campaign, the average aerosol concentration was 11 μg m^{-3}. Compared with monitoring data from the IMPROVE network, the organic component made up a large fraction of total mass, varying from 70% in clean air to 40% in high concentration sulfate plumes. In combination with other optical and chemical measurements, the AMS gave information on secondary organic aerosol (SOA) production and the time evolution of aerosol light absorption. CO is taken as a conservative tracer of urban emissions and the ratios of organic aerosol and aerosol light absorption to CO examined as a function of photochemical age. Comparisons were made to ratios determined from surface measurements under conditions of minimal atmospheric processing. In air masses in which the NO_x to NO_y ratio has decreased to 10%, the ratio of organic aerosol to CO has quadrupled indicating that 75% of the organic aerosol is secondary. Also, the ratio of light absorption to CO has more than doubled, which is interpreted as an equivalent increase in the light absorption efficiency of black carbon due to aerosol ageing.

Citation: Kleinman, L. I., et al. (2007), Aircraft observations of aerosol composition and ageing in New England and Mid-Atlantic States during the summer 2002 New England Air Quality Study field campaign, *J. Geophys. Res.*, *112*, D09310, doi:10.1029/2006JD007786.

1. Introduction

[2] High concentrations of aerosol particles occur over most of the eastern USA. These particles reduce visibility, have adverse health impacts, and interact with the climate system, either directly by reflecting and absorbing sunlight, or indirectly by modifying cloud properties [*North American Research Strategy Tropospheric Ozone*, 2003].

[3] Major constituents of $PM_{2.5}$ (particles with aerodynamic diameter smaller than 2.5 μm) in industrialized regions are the inorganic salts of SO_4^{2-}, NH_4^+, and NO_3^-, organic compounds, black carbon (BC), crustal material, and associated water. Organic compounds are subdivided into primary and secondary organic aerosol (POA and SOA) according to whether they are directly emitted or formed in the atmosphere through gas to particle conversion. Often, 85% or more of dry $PM_{2.5}$ mass can be accounted for by $NH_4^+ - SO_4^{2-} - NO_3^-$ salts and organic compounds [*Malm et*

[1] Atmospheric Sciences Division, Brookhaven National Laboratory, Upton, New York, USA.
[2] Atmospheric Science Department, Pacific Northwest National Laboratory, Richland, Washington, USA.
[3] Brechtel Manufacturing Inc., Hayward, California, USA.
[4] Aerodyne Research Inc., Billerica, Massachusetts, USA.

0148-0227/07/2006JD007786$09.00

al., 2004]. This is especially true for particles with diameter smaller than 1 μm, which eliminates much of the crustal component.

[4] Aerosol chemical and microphysical properties have been measured in a diverse array of chemical regimes ranging from pristine ocean basins to urban street corners. It is more difficult to determine the time evolution of these properties, especially for the formation of the organic aerosol component. As a result, most current aerosol models use parameterizations derived from smog chamber studies [e.g., *Griffin et al.*, 2002] that have not been fully tested against atmospheric observations. There are studies that provide evidence that the current picture of SOA production is incomplete. For example, *Brock et al.* [2003] have inferred SOA production in SO_2 containing plumes from petrochemical facilities in Houston severalfold greater than expected and *de Gouw et al.* [2005] have measured organic aerosol concentrations off the east coast of New England in excess of that predicted from measured VOCs. *Volkamer et al.* [2006] observed rapid SOA production in Mexico City with a yield much greater than could be explained.

[5] This study reports results from the DOE G-1 during the summer of 2002 New England Air quality Study (NEAQS) field campaign. Seventeen research flights were conducted in New England and Middle Atlantic States; a region with a diverse and dense array of urban, industrial, and utility sources of aerosols and aerosol precursors. This campaign was the second aircraft deployment of the Aerodyne aerosol mass spectrometer (AMS); the first being a deployment in ACE-Asia reported by *Bahreini et al.* [2003]. Mass spectrometers, in general, and the AMS in particular, have opened up new areas of inquiry by allowing for the rapid quantification of size resolved chemical composition. Rapid response is essential for aircraft applications. At typical flight speeds of 100 m s^{-1}, pollutant features that are of order 5 km in width translate into a 50 s signal in the time domain. By allowing for measurements that cover a large geographic area with sufficient time resolution to follow composition changes, aerosol mass spectrometers have the potential to provide much needed kinetic information on the time evolution of organic aerosols. But, compared to ground sites, aircraft represent a challenging environment for the AMS. In addition to the requirement that response times be an order of magnitude faster than is typical for measurements at the surface, instrument performance is degraded because power to maintain a high vacuum in the AMS is generally not available between flights. Nevertheless, we were able to obtain 30 s concentration measurements which had a high signal-to-noise ratio for all except the cleanest air masses.

[6] Our analysis of the 2002 NEAQS data set consists of an evaluation of the performance of the AMS and a description of aerosol observations with an emphasis on SOA formation and aerosol light absorption. AMS volumes and size spectra are compared with those determined from a Passive Cavity Aerosol Spectrometer (PCASP) (optical particle counter) and a Twin Scanning Electrical Mobility Spectrometer (TSEMS). Mie scattering calculations are used to determine total scattering at 550 nm from the AMS, PCASP, and TSEMS which are compared with that observed from an integrating nephelometer. The AMS measurements have a median bias of +25% (33% with an estimated refractory component) and +18% relative to TSEMS volume and measured scattering, respectively. AMS results have been corrected for an acid-dependent collection efficiency which is derived from the relation between the AMS and PCASP volume in two high concentration SO_4^{2-} plumes.

[7] A second focus of this study is to characterize the abundance and formation processes of organic aerosol and changes in aerosol light absorption. Aerosol measurements from the RV Ron Brown during the 2002 NEAQS campaign demonstrate that a surprisingly high fraction of aerosol mass is due to organics [*Bates et al.*, 2005] and that the source of this organic mass cannot be identified with our current understanding of organic aerosol production [*de Gouw et al.*, 2005]. The greater spatial coverage of our measurements and their midboundary layer altitude helps put the ship board observations in a broader geographic context. In this study SOA production was investigated by examining the ratios of organic aerosol and light absorption to CO, where CO is a conservative tracer of urban emissions. These ratios were compared with literature values appropriate for fresh emissions. By examining the organic to tracer ratio as a function of photochemical age (NO_x/NO_y), we obtain information on the rate of SOA production. Changes in light absorption per unit BC due to atmospheric ageing processes are inferred from the time evolution of the ratio of aerosol light absorption to CO.

2. Field Campaign

[8] As part of the NEAQS campaign, the DOE G-1 aircraft conducted 17 research flights between 10 July and 11 August 2002. Figures 1a and 1b show composite flight tracks covering daytime and nighttime hours. Daytime flights were planned for a regional survey of aerosol precursors, composition, and microphysical properties. Our geographic focus was on southern New England and the Mid-Atlantic States. Nighttime sampling was primarily done in the vicinity of the Boston urban plume to follow chemical transformations [*Zaveri et al.*, 2004]. Flight altitude was mostly at midboundary layer (or midresidual layer) altitude between 350 and 1000 m above the surface. A time series of aerosol concentration is presented in Figure 2 as an introduction to the data set. A wide range of pollutant conditions were encountered, ranging from very clean air following a frontal passage (10 July and 7 August) to high concentration events covering multistate regions (14 July and 21 July). Aerosol concentrations are summarized in Table 1.

3. Experimental Procedure

3.1. Aerosol Mass Spectrometer

[9] An Aerodyne aerosol mass spectrometer (AMS) was used to determine the composition and size distribution of ambient aerosol. There are several dozen such instruments in use, resulting in many publications that describe principles of operation and issues of data reduction and data quality [e.g., *Jayne et al.*, 2000; *Allan et al.*, 2003a, 2003b; *Jimenez et al.*, 2003]. We confine our discussion here to aspects that are pertinent to understanding the G-1 AMS

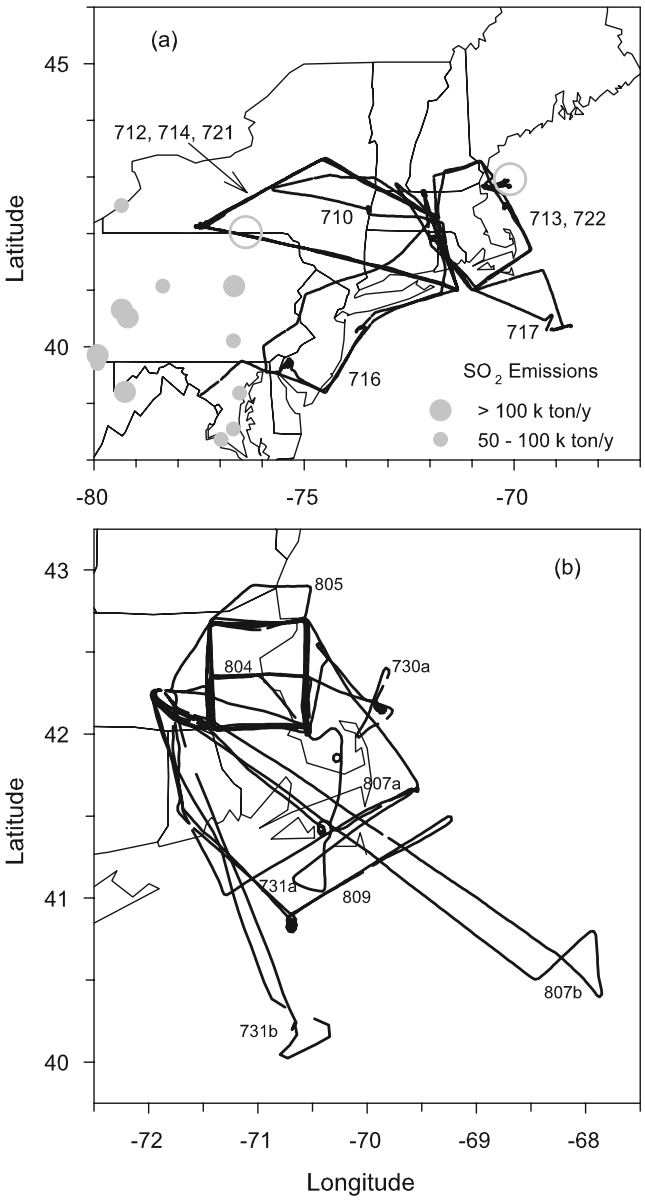

Figure 1. Ground track of G-1 for (a) daytime and (b) nighttime flights. Flights are identified by month and day with "a" and "b" denoting the first and second flights on the same day. Locations of high-concentration acidic plumes discussed in text identified with an open circle on 721 and 722 ground tracks.

data set and its relation to concurrent observations of light scattering and particle size spectra.

[10] Ambient air enters the G-1 through a two stage diffuser inlet which supplies air to the AMS, nephelometer, particle soot absorption photometer (PSAP), and TSEMS. From inlet to detector an aerosol particle in the AMS encounters the following units: (1) critical orifice, (2) aerodynamic lens, (3) skimmer separating the lens from a high vacuum chamber, (4) chopper wheel, (5) heated collector surface, (6) electron beam ionizer, and (7) quadrapole mass filter (see for example, Figure 1 of *Jayne et al.* [2000] or Figure 1 of *Jimenez et al.* [2003]).

[11] The AMS cycles between two modes, which differ according to whether the particle beam is being chopped or not. In the TOF (time of flight) mode, the beam is chopped and particles are sized according to their transit time between the chopper and heated collector surface. Size-dependent particle velocities are acquired as ambient air expands through a nozzle into a vacuum chamber [*Allan et al.*, 2003a]. For spherical particles, as assumed in this study, the vacuum aerodynamic diameter measured by the AMS is related to geometric diameter and density, ρ, by

$$D_p(\text{geometric}) = D_{va}(\text{vacuum aerodynamic})/(\rho/\rho_0) \quad (1)$$

where ρ_0 is the density of water. *DeCarlo et al.* [2004] and *Slowik et al.* [2004] discuss the effects of (nonspherical) particle shape on vacuum aerodynamic diameter, which yields an underestimate of vacuum aerodynamic diameter and an overestimate of mobility diameter. These effects are most pronounced for highly irregular fresh soot particles and are expected to be of minimal importance for the more aged organic–sulfate–ammonium mixtures seen during NEAQS 2002. The diameter range of the AMS is determined by the focusing properties of the aerodynamic lens. Transmission efficiencies are 100% for particles with vacuum aerodynamic diameters between 60 and 600 nm, decreasing to zero at 2000 nm [*Jayne et al.*, 2000]. When the chopper is fixed in the open position (MS mode) an increased number of mass units are scanned and particles of all sizes are detected. The AMS analysis software [*Allan et al.*, 2004] determines concentration from the MS mode and partitions that concentration into size bins using TOF measurements. For most flights, the sample averaging time was 30 s split between MS and TOF modes. The detection limit for a 30-s measurement period (after three point smoothing) was estimated as the standard deviation of concentration in all of the clean air periods during the campaign. A criteria of PCASP volume less than 0.5 μm^3 cm^{-3} yielded 163 measurement periods with standard deviations of 0.09, 0.14, 0.05, 0.6, and 0.6 μg m^{-3} for SO_4^{2-}, NH_4^+, NO_3^-, organics, and total aerosol, respectively. Size spectra are much nosier, which is an unavoidable consequence of the poor counting statistics in a TOF measurement period. Even with additional smoothing in the size domain, a 30-s spectrum can contain unrealistic peaks and valleys, including negative concentrations.

[12] Measurement of aerosol components depends on the aerosol impinging on a heated collector surface after which it is vaporized, ionized, and detected by a quadrapole mass filter. In typical applications, as on the G-1, the temperature of the collector surface is 600–650°C, adequate to vaporize mixed SO_4^{2-}–NO_3^-–NH_4^+ salts and organic compounds which together constitute most of the mass in the submicron size range. The signal at mass unit 44 (M44) contains the CO_2^+ fragment from oxidized hydrocarbons and has been used as a surrogate for aged organic aerosol [*Alfarra et al.*, 2004; *Zhang et al.*, 2005a]. Refractory materials such as NaCl, mineral dust, or black carbon are not detected by the AMS.

[13] Quantification of components depends on ionization efficiency (IE) and collection efficiency (CE), defined here as particles that reach the AMS collector divided by particles transmitted by the aerodynamic lens. Calibration

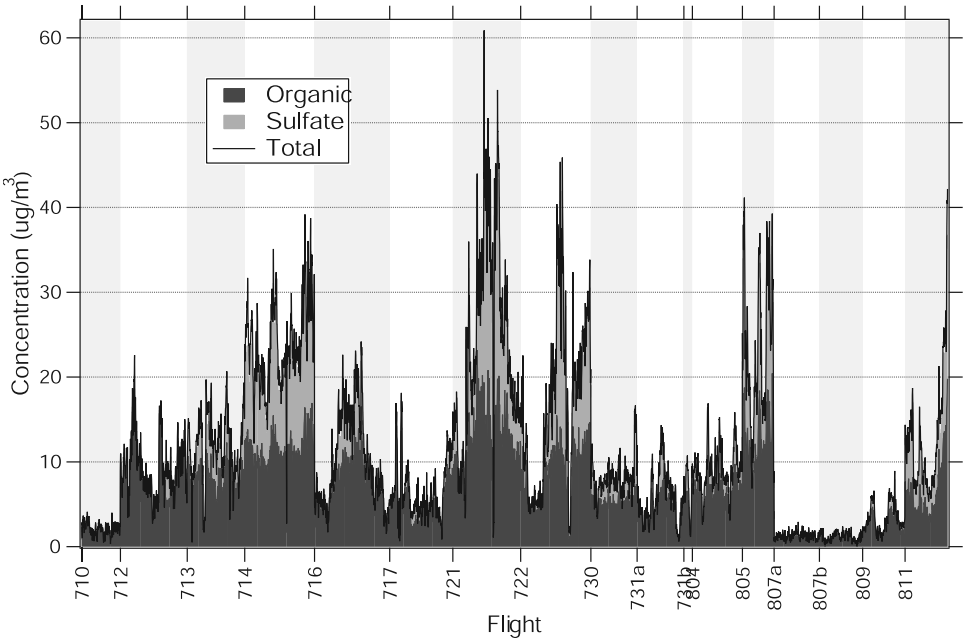

Figure 2. Time series of total aerosol concentration and organic and sulfate components. Time breaks between flights occur at boundaries of vertical stripes. The second flight on 31 July (731b) appears short because the AMS measurement period was 120 s, approximately four times longer than other flights.

experiments indicate that the IE of organics, relative to NO_3, ranges between 1.9 for freshly formed organic combustion products to 1.3 for aged oxygenated species [*Jimenez et al.*, 2003]. In this study an IE of 1.4 was used, on the assumption used by *Zhang et al.* [2005b] and *de Gouw et al.* [2005] that accumulation mode particles contain mainly oxidized organics.

[14] CE values smaller than one have been attributed to particle beam spread and particle bounce [*Salcedo et al.*, 2005]. Beam spread is thought to reflect the aerodynamics of nonspherical particles. Particle bounce occurs when less liquid-like particles rebound off of the heated collector surface, hence not contributing to the mass spectrometer signal. Collection efficiencies have been derived from laboratory experiments and field comparisons with colocated instruments. These are bulk collection efficiencies that do not provide size dependence information. *Zhang et al.* [2005c] use a CE of 0.5 for inorganic constituents and 0.7 for organics, the latter value representing an average of 0.5 for internally mixed accumulation mode organics and 1.0 for an external mixture of sooty combustion products. *Allan et al.* [2004], *Salcedo et al.* [2005], and *Takegawa et al.* [2005] use a CE of 0.5 for all constituents; *Drewnick et al.* [2004] and *Weimer et al.* [2006] use a CE of 0.42–0.43. *Alfarra et al.* [2004] operated two AMS instruments at nearby sites and found CEs of 0.5 and 1.0 under conditions of low and high RH, respectively. The low RH limit is more appropriate for our measurements because sample air is heated above ambient temperature. A comparison of AMS and PILS (Particle Into Liquid Sampler) data (T. Onasch, personal communication) indicates that CE has a value near 0.5 for particles less acidic than $(NH_4)HSO_4$ rising to 1 as the $[NH_4^+/SO_4^{2-}]$ ratio decreases in order to account for the higher sticking probability of more liquid, acidic particles. In this study we used

$$\begin{aligned} &\mathrm{CE} = 0.5 \text{ for } \left[\mathrm{NH_4^+}\right]/\left[\mathrm{SO_4^{2-}}\right] \geq 1 \\ &\mathrm{CE} = 1 \text{ for } \left[\mathrm{NH_4^+}\right]/\left[\mathrm{SO_4^{2-}}\right] \leq 0.75 \\ &\mathrm{CE} = 0.5 + 2\left(1 - \left[\mathrm{NH_4^+}\right]/\left[\mathrm{SO_4^{2-}}\right]\right) \text{ for } 0.75 < \left[\mathrm{NH_4^+}\right]/\left[\mathrm{SO_4^{2-}}\right] < 1 \end{aligned} \quad (2)$$

where square brackets indicate molar concentration. The linear increase from CE = 0.5 to CE = 1 is based on a comparison between PCASP and AMS volumes in acidic plumes shown in a following section. In almost 90% of our measurements, particles are more basic than $(NH_4)HSO_4$ and therefore the main effect of the CE correction is to multiply concentrations by (1/0.5) = 2. Aerosols more acidic than $(NH_4)HSO_4$ will be referred to as "acidic".

[15] Although the dependence of CE on acidity can explain variations in AMS measurements vis-à-vis other instruments, it is probable that acidity itself is only a qualitative descriptor for particle phase inside the AMS, which depends on hygroscopicity and can be affected by many aerosol constituents. It is also possible that CE depends on particle size, an effect not generally considered.

Table 1. AMS Aerosol Composition

	Concentration (μg m^{-3})				
Data Subset	Organic	SO_4^{2-}	NH_4^+	NO_3^-	Total
<10 μg m^{-3}	3.6	0.9	0.3	0.2	5.0
>30 μg m^{-3}	14.3	17.1	2.9	0.7	35.0
All	6.5	3.4	0.8	0.4	11.1

Table 2. Refractive Index and Density of Aerosol Components

Compound	Refractive Index	Density (g cm^{-3})
NH_4NO_3	1.55	1.77
H_2SO_4	1.41	1.80
$(NH_4)HSO_4$	1.48	1.78
$(NH_4)_2SO_4$	1.53	1.76
Organics	1.55	1.2[a]

[a] *Turpin and Lim*, 2001.

[16] AMS data will be compared with volume measurements from the PCASP and scattering measurements from the nephelometer. In order to conduct these comparisons we make use of aerosol density and refractive index which are determined from the component values listed in Table 2. Concentrations of NH_4NO_3, $(NH_4)_2SO_4$, $(NH_4)HSO_4$, and H_2SO_4 are calculated from measurements of NH_4^+, NO_3^-, and SO_4^{2-}. Volumes of each component were determined from the measured mass and the densities in Table 2. Component volumes are added to get the total volume. The ratio of total mass to total volume yields the density of the mixture. Refractive index was arrived at by using the component values in Table 2, combined according to volume fraction. Because we are limited by the composition information derived from the AMS, the determination of density and refractive index does not take into account the presence of refractory material. On the basis of surface measurements of $PM_{2.5}$ from the IMPROVE network [*Malm et al.*, 2004] and observations of PM_1 in the Gulf of Maine [*Bates et al.*, 2005], we estimate that the refractory component is 10% of aerosol mass and approximately 6% of its volume.

[17] Density and refractive index have been calculated only as a function of time rather than as a function of time and particle size. The former procedure requires the assumption that the proportions of component species do not vary over the AMS size range, but has the considerable advantage of not requiring size spectra. As shown in the following section, the campaign average size spectra for organic and ionic constituents are similar suggesting that aerosols are internally mixed and therefore can be described by a size-independent density and refractive index. Neglecting the size dependence of density could lead to a distortion in the size spectra when equation (1) is used to convert from vacuum aerodynamic diameter to geometric diameter but will not affect the determination of aerosol volume from aerosol mass and composition.

3.2. PCASP

[18] An optical particle probe (PCASP-100X, Particle Metrics Inc., Longmont, CO) mounted on a pylon near the nose of the aircraft was used to determine the number concentration of aerosol particles in 15 size bins covering the nominal size range $D_p = 0.1–3$ μm which captures most of the mass and scattering in the accumulation mode. Data from the first third of one flight on 14 July were not useable. Heat from a deicing unit and from adiabatic compression evaporates water from the ambient aerosol [*Haller et al.*, 2006]. Calibration of the PCASP was performed by the manufacturer prior to the field campaign using polystyrene microspheres. Size bins of the PCASP were corrected for the difference in refractive index between polystyrene ($m = 1.59$) and ambient aerosol using the response curves of *Liu and Daum* [2000]. The refractive index of the ambient aerosol was determined from AMS measurements of SO_4^{2-}, NH_4^+, NO_3^- and organics as described above. Aerosol volumes determined using the corrected size bins are on average 17% greater than the uncorrected values.

3.3. TSEMS (Differential Mobility Analyzer)

[19] Particle number size distributions ($D_p \sim 5–530$ nm) were measured with a Twin Scanning Electrical Mobility Spectrometer (TSEMS) [*Buzorius et al.*, 2004]. This instrument consists of two units operating in parallel, each with a DMA (Differential Mobility Analyzer) to sort charged particles according to mobility in an applied electric field and a CN counter to determine number concentration. Mobility diameters between 5 and 80 nm and 40 and 530 nm were covered by a Nano-DMA (TSI 3085, St. Paul, MN) and a Long-DMA (TSI 3081), respectively. A pair of size spectra is generated by exponentially ramping the DMA voltage in alternate directions. Up scans and down scans which together typically took 2.5 min were averaged. Data postprocessing included inversions of raw counts for smearing effects and multiply charged particles and accounted for particle losses in sampling lines [*Collins et al.*, 2002].

[20] In this study we report aerosol volumes and scattering which are due almost entirely to aerosol particles measured by the Long-DMA, which henceforth will be referred to as "DMA" measurements. A Nafion diffusion dryer reduced the RH to below a measured value of 25%, at which point residual water can be ignored. It is assumed that a particle's geometric diameter is equal to its measured mobility diameter, as is the case for spherical particles.

[21] As part of the DMA data reduction procedure, a correction factor is determined that accounts for a small contribution to the measured signals coming from larger multiple charged aerosol particles. In this procedure the concentrations of particle between 500 and 1000 nm are estimated by fitting a Gaussian function to the accumulation mode. In several comparisons between instruments we will use volume and scattering determined from the DMA that includes an estimated contribution from 500–1000 nm size particles. These data are presented alongside data that are derived from the 5–500 nm observed size range so that effects of the extrapolation to a larger size range can be judged.

[22] Because of startup and shutdown procedures, DMA data are often missing from the first and last 5–15 min of each flight. In addition, DMA data are not available for 3 of 17 flights: 10 July and two flights on the late night and early morning of 6 and 7 August.

3.4. Nephelometer and Scattering Calculations

[23] A TSI 3563 integrating nephelometer was used to determine total aerosol light scattering at 550 nm, referred to here as b_{SP}. The aircraft inlet has a 50% cutoff near 1.5 μm [*Brechtel*, 2003]. A heater upstream of the nephelometer maintains an inlet temperature of 40°C which typically reduces RH by 70–80% and removes almost all particle-bound water. Scattered photons are not uniformly detected by the nephelometer because of variations in angular sensitivity including a blind spot in the near-forward direction. *Anderson and Ogren* [1998] give a correction factor for

these nonidealities. Using that algorithm, we have corrected the nephelometer signal which resulted in an average scattering increase of 8%.

[24] A Mie scattering code was used to determine total scattering at 550 nm based on size spectra determined from the AMS, PCASP, and DMA and refractive index determined from AMS composition measurements. Sensitivity calculations showed that scattering determined from the PCASP had only a minimal dependence on refractive index. Size determination in the PCASP is based on a light scattering signal, similar to that used by a nephelometer. Refractive index affects the size bin correction in a way that is almost canceled by the dependence of light scattering on refractive index. Calculated scattering was insensitive (<2% effect) to the inclusion of particles between 1.2 and 2 μm diameter.

3.5. PSAP

[25] A Particle Soot Absorption Photometer (PSAP, Radiance Research) was used to measure aerosol light absorption at a wavelength of 567 nm. Filters were changed to keep transmission above 75%. PSAP signals were corrected to correspond to the calibration and scattering response determined by *Bond et al.* [1999], resulting in an average absorption decrease of 30% relative to uncorrected values.

3.6. Gas Phase

[26] For this study we make use of trace gas measurements of NO, NO_2, NO_y, and CO. Nitrogen oxides are detected by the chemiluminescent reaction of NO with O_3; NO_2 is photolyzed to yield NO, and NO_y is reduced to NO by a 350°C Mo catalyst. A detailed description of the NO_x detector is given by *Springston et al.* [2005]. CO was measured by resonance fluorescence in the vacuum UV [*Volz and Kley*, 1985] using an instrument manufactured by Resonance Ltd., Barrie, ON, Canada. Baseline subtraction of background was done by selectively removing CO using Sofnocat catalyst. The 1σ precision was 5 ppbv for a 2-s measurement.

3.7. General

[27] Values for aerosol concentration, scattering, and absorption are all adjusted to ambient conditions of temperature and pressure (values at sea level and 298°K would on average be 10% lower). Particle size is given as the geometric diameter of the dried aerosol. The abundance of gas phase species is expressed as a volume-mixing ratio, i.e., parts per billion. Eastern Standard Time (EST) equal to UTC minus 5 hours is used to identify measurement periods. Flights, however, are identified by their UTC start time in order to have the dates match those on our FTP site (ftp://ftp.ecd.bnl.gov/pub). Measurements have been put on a time base defined by the AMS measurement cycle. This time base is approximately 30 s long with one exception on 31 July where the AMS had a 120-s measurement cycle. Variables on the AMS time base were subject to a 3-point binomial smoothing [i.e., $V(t_n) = V(t_{n-1}) + 2\ V(t_n) + V(t_{n+1})$].

4. Volume and Scattering Comparisons

[28] We have intercompared volumes derived from the AMS, PCASP, and DMA and compared total scattering calculated from the AMS, PCASP, and DMA with that measured by the nephelometer. Our main interest is in examining the AMS data since (1) there are known uncertainties in quantifying AMS measurements, (2) the necessity for rapid time response in aircraft operations compromises the signal-to-noise ratio of AMS measurements, and (3) the primary results from this study, outside of the instrument intercomparison, are from the AMS measurements.

Table 3. Median Contribution of Small and Large Particles to Total Volume

Measurement	% Volume, D_p < 100 nm	% Volume, D_p > 500 nm
AMS	5.3	14.0
PCASP	Not applicable	4.9
DMA	4.6	13.7[a]

[a]DMA volume from particles with D_p > 500 nm is an extrapolation from a fitted spectra.

[29] Ideally, we would like to restrict the comparisons between these four instruments to accumulation mode particles. Each instrument makes measurements over a different size range. Therefore comparisons have been carried out over two size ranges. The first is 100–500 nm which is covered by the three particle sizing instruments, although there is some fall-off in transmission efficiency near 500 nm for the AMS. The second size range is our best approximation to the full accumulation mode. For the DMA it consists of the entire measured size range (the volume from Aitken size particles is small and their scattering is negligible) plus the spectrum that was extrapolated to 1000 nm. For the AMS we use the full measured size range. The PCASP data are from particles with D_p between 100 and 1200 nm to which we add a sub 100-nm contribution to volume as determined from the DMA. An upper bound of 1200 nm was selected because the PCASP volume spectrum typically has a deep minimum near this diameter with a coarse particle mode occurring at larger diameters. Contributions of particles with D_p < 100 nm and D_p > 500 nm to total volume are given in Table 3.

[30] Volume and scattering comparisons are shown in Tables 4 and 5. Data in these tables are based on 72% of 5694 AMS measurement periods in the campaign, the selection criterion being that there are simultaneous AMS, PCASP, DMA, and nephelometer observations. Equation (2) was used to correct the AMS data for an acid dependent CE, as described in section 5. The figures of merit used to judge a comparison are the median value of a ratio and the interquartile range of that ratio expressed as a percentage of the median. The ordering of the data sets based on the 1000 nm DMA data is

$$\text{PCASP} < \text{Nephelometer} \approx \text{DMA} < \text{AMS} \tag{3}$$

[31] Differences in median ratios are comparable or smaller than one would expect based on instrument uncertainties. As a general indication of expectations, the intercomparison and error analysis of *Moore et al.* [2004] yielded a 50% uncertainty in PCASP derived volume. *Haller et al.* [2006] report a comparison between a PCASP and nephelometer essentially identical to that reported here. They find that a 1/2 channel uncertainty in the PCASP yields a 30% uncertainty in

Table 4. Volume Comparisons Between AMS, DMA, and PCASP

	D_p = 100–500 nm, Median ((75th–25th)/50th)[a]		D_p = total range[b], Median ((75th–25th)/50th)[a]	
Volume Ratio	Data Points[c]	Flights[d]	Data points[c]	Flights[d]
DMA/PCASP	1.04 (31%)	1.04 (15%)	1.15 (32%)	1.15 (20%)
AMS/PCASP[e]	1.32 (53%)	1.28 (26%)	1.47 (32%)	1.44 (15%)
AMS/DMA[e]	1.26 (58%)	1.20 (33%)	1.25 (48%)	1.18 (35%)

[a]Interquartile range of ratio in 1st column as a percent of median value.
[b]PCASP total volume = volume from 100–1200 nm measured by the PCASP plus volume from 40–100 nm measured by the DMA. DMA volume is from 40–1000 nm. The portion below 500 nm is measured and the portion above 500 nm is estimated by assuming a Gaussian fit to the accumulation mode. AMS volume is affected by a decreasing transmission efficiency above 500 nm.
[c]4074 data points with simultaneous AMS, PCASP, DMA, and nephelometer observations.
[d]14 data points, each one being the median value of a ratio on a single flight.
[e]AMS volume does not include a refractory component estimated to be 6%.

calculated scattering. Other groups, however, have reported better agreement [*Quinn et al.*, 2002; *Bates et al.*, 2005]. Volumes derived from the DMA have an uncertainty of about 25%, with the largest contribution from charging efficiency. The accuracy of AMS measurements has been quantified by comparisons with colocated instrument [*Drewnick et al.*, 2003; *Takegawa et al.*, 2005; *Weimer et al.*, 2006]. These comparisons indicate an AMS accuracy of ~25% for major ions and organics. Reported collection efficiencies were 0.42 to 0.5 with little variation during a measurement campaign. Volumes deduced from AMS observations reported in this study are estimated to have a low bias of 6% due to refractory aerosol and a few percent low bias due to decreased transmission at the high end of the 100–500 nm size window used for comparisons with the PCASP and DMA.

[32] Table 4 indicates a wide variation in the spread of ratios (interquartile range expressed as a percentage of the median) with the lower numbers indicating higher correlations between numerator and denominator. Comparisons involving the DMA tend to have lower correlations. An inspection of time series data shows cases where the longer data integration period of the DMA causes it to miss rapidly changing features. By far the best correlation is for the light scattering comparison between the PCASP and nephelometer. Plots of PCASP volume and scattering versus measured b_{SP} are shown in Figure 3. Note the many stranded appearance of the volume-scattering plot which is due to differences in particle size. Scattering per unit volume varies by about a factor of 2. The calculated scattering versus b_{SP} data points in Figure 3b collapse to a single line as the Mie scattering calculation correctly accounts for the particle size dependence of the volume-scattering relation. In the PCASP, particles are sized and counted by light scattering, similar to the nephelometer. The commonality of method contributes to the excellent correlation.

[33] Figure 4 shows a comparison between scattering calculated from the AMS and that measured from the nephelometer. Compared with the PCASP-b_{SP} relation shown in Figure 3b, there is much more scatter in the AMS-b_{SP} relation. Two factors have to be considered in

Table 5. Comparison of Total Scattering at 550 nm Measured With the Nephelometer and Calculated From PCASP, DMA, and AMS Size Distributions

Scattering Ratio	Median ((75th–25th)/50th)[a]
PCASP/nephelometer	0.73 (12%)
DMA(500)/nephelometer[b]	0.81 (36%)
DMA (1000)/nephelometer[c]	1.02 (37%)
AMS/nephelometer	1.18 (48%)

[a]Interquartile range as a percent of median value.
[b]Measured DMA spectra below 500 nm used in ratio.
[c]DMA includes extrapolated spectra between 500 and 1000 nm.

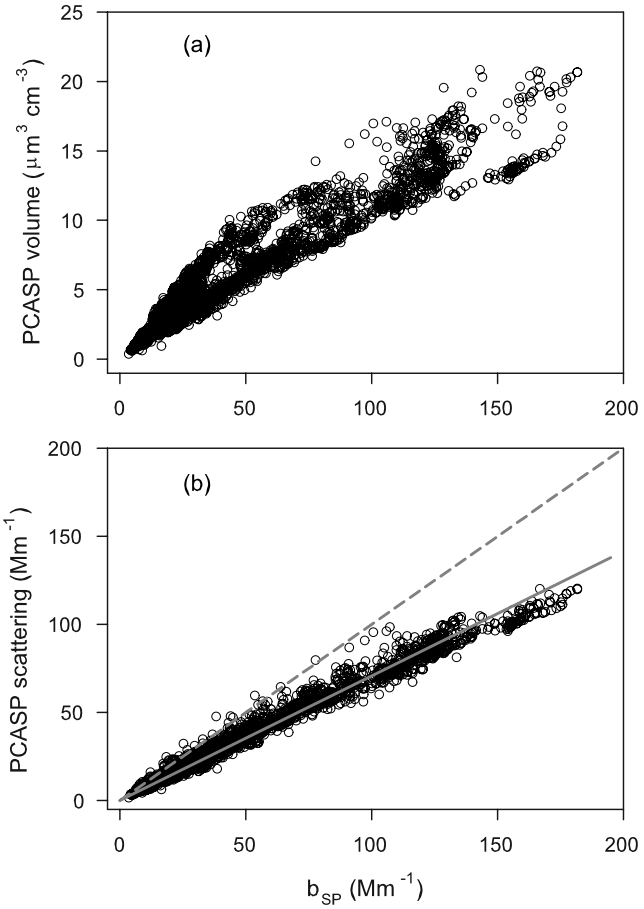

Figure 3. PCASP (a) volume and (b) calculated scattering versus total scattering from nephelometer at 550 nm. Units for scattering are inverse mega meters. The linear least squares regression line in Figure 3b is constrained to pass through the origin and has a slope of 0.71with an r^2 = 0.98. Dashed line is 1 to 1.

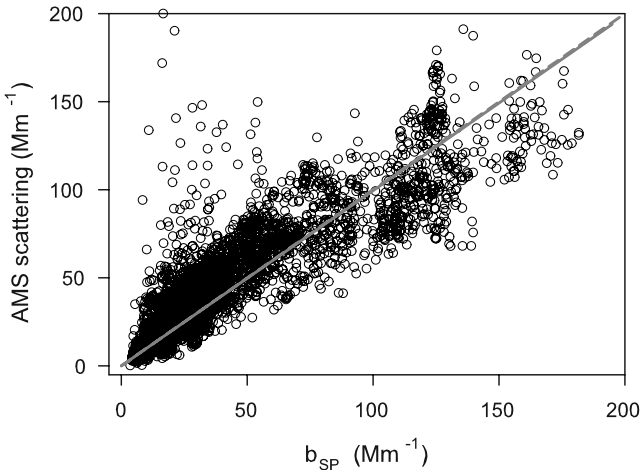

Figure 4. Scattering at 550 nm calculated from AMS spectra versus that measured from the nephelometer. Outliers with calculated scattering > 200 Mm^{-1} omitted from graph and regression statistics. Linear least squares regression line through origin has slope = 0.99 and r^2 = 0.69. Dashed line is 1 to 1. A small number of points with negative calculated scattering inadvertently omitted. These points do not effect the median and interquartile range reported in Table 5.

understanding this scatter. First, is the difficulty of determining a size spectrum from a 30-s AMS measurement. Second, is the fact that unlike the PCASP, particles are not sized and counted by light scattering. If a particle has a nonspherical geometry or has refractory components, the PCASP and nephelometer will respond in a similar fashion but errors will be introduced into the AMS-nephelometer scattering comparison.

[34] Figure 5 shows a volume comparison between the AMS and PCASP for the entire accumulation mode and for the size range 100–500 nm. Regression slopes for comparisons between the AMS and other instruments are somewhat closer to unity than the median ratios shown in Tables 4 and 5 as there is better agreement for the high concentration points which contribute disproportionately to regression statistics. The correlation exhibited in Figure 5 is comparable to that found in other studies, despite the fact that measurement periods are an order of magnitude shorter than is typical for surface-based instruments [see for example, *Zhang et al.*, 2005c]. There is increased scatter when the AMS-PCASP comparison is restricted to 100–500 nm. As with the AMS scattering results shown in Figure 4, the volumes from 100–500 nm are derived from size spectra based on small numbers of particles counted in TOF mode, which are subsequently normalized to total concentration determined in MS mode. As extreme examples of the resulting peaks and valleys which can appear in the size spectra, Figure 5b contains data points in which the 100–500 nm volumes are either negative or greater than total volume. It is because of these extreme outliers that we have used medians and interquartile ranges rather than regression statistics for instrument comparisons.

[35] Part of the spread in the interquartile ranges listed in Tables 4 and 5 is due to instrument precision and variations in aerosol properties; part is due to flight to flight changes in instrument performance. The latter source of variability has been qualitatively addressed by repeating the calculation of volume ratios in Table 4 using median DMA/PCASP, AMS/PCASP, and AMS/DMA volume ratios determined for each of 14 flights. From this data set one gets campaign medians that are similar to those obtained from the original data set in which each measurement period is an independent observation. However, the spread in ratios (again defined as the interquartile range divided by median value) has decreased. If errors are taken to be independent (i.e., can be added in quadrature), a comparison of the "data point" and "flight" spreads shows that flight to flight variability accounts for about 1/4 (AMS/PCASP) to 1/2 (AMS/DMA) of the total variability. Some of this variation is due to true changes in instrument performance but part may be due to a coupling between the response to different aerosol types and flight to flight changes in prevalence. An example of the latter effect is the variable number of acidic plumes encountered on each flight. In this case, acidity is taken into account (albeit,

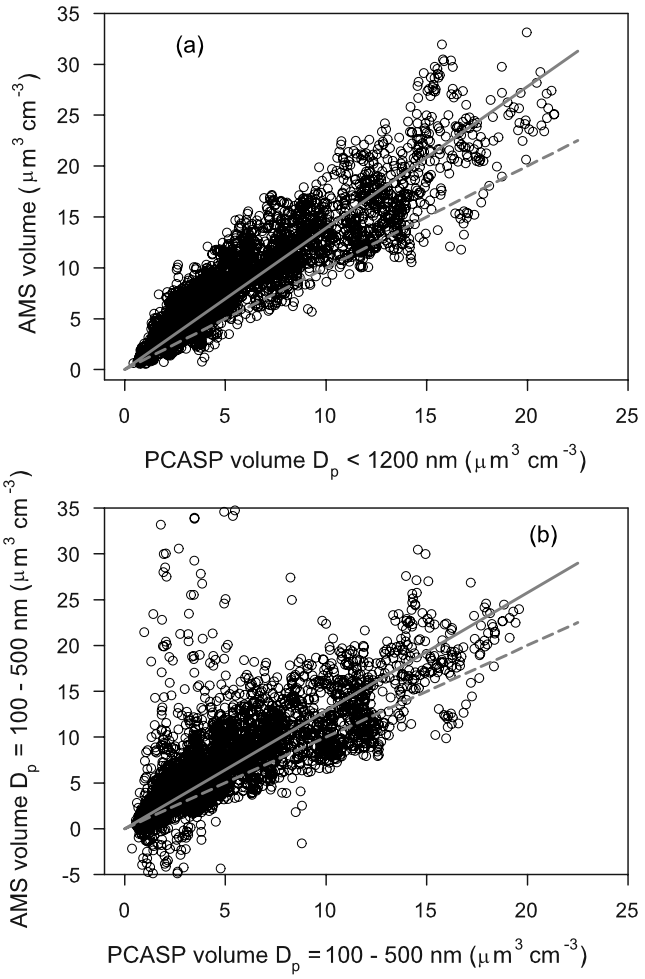

Figure 5. AMS versus PCASP volume. Dashed lines are 1 to 1. (a) Entire AMS spectra, PCASP = 100–1200 nm plus DMA volume below 100 nm. Linear least squares regression line through origin has slope = 1.39 and r^2 = 0.82. (b) AMS and PCASP volume for D_p = 100–500 nm. Outliers with AMS volume > 35 or < −5 μm^3 cm^{-3} omitted from graph and regression statistics. Linear least squares regression line through origin has slope = 1.29 and r^2 = 0.54.

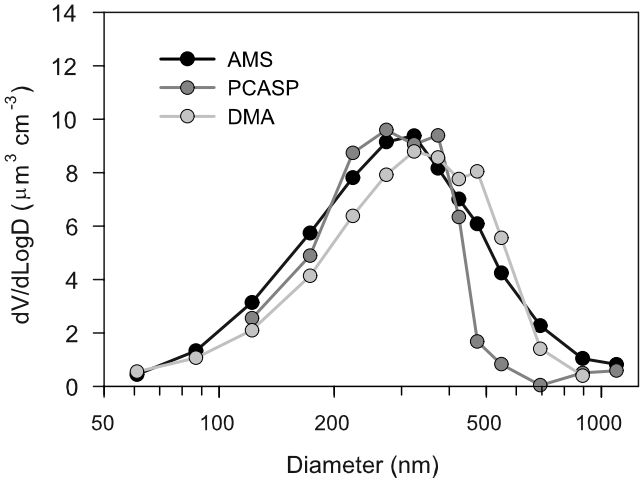

Figure 6. Size spectra calculated from median value of $dV/d\mathrm{Log}D_p$ as a function of D_p for the AMS, PCASP, and DMA. Spectra use all time periods with coincident AMS, PCASP, and DMA observations. Last three points of DMA spectra have $D_p > 500$ nm and are from an extrapolation. The AMS spectrum has been normalized using the median AMS/DMA volume ratio in Table 4, i.e., AMS volumes are divided by 1.25.

imperfectly) by a variable CE according to equation (2). Because of the limited number of acidic samples, the overall contribution to explaining the variance in the volume ratios is minor.

[36] In Figure 6 we compare volume size spectra, $dV/d\log D_p$, for the PCASP and DMA, with an AMS spectrum normalized as described in the figure caption. All three instruments have similar volume distributions below 400 nm. Above 400 nm, the PCASP volumes decrease rapidly, an effect that we had previously noted with this instrument [*Springston et al.*, 2005]. Between 400 and 700 nm there is a Mie scattering ambiguity which leads to the possibility that particles are mis-sized [*Leaitch and Isaac*, 1991]. AMS and DMA volume distributions have the same shape for particles larger than 500 nm but this may in part be coincidental as the DMA results are extrapolations in this size range and the AMS has decreased transmission efficiency [*Jayne et al.*, 2000].

5. High SO_4^{2-} Plumes With Variable CE

[37] The NEAQS data set contains two measurement periods in high concentration SO_4^{2-} plumes in which a comparison of AMS aerosol concentration with other measurements gives clear evidence of a variable CE. The first of these plumes was encountered on 21 July at the NY-PA border. Back trajectories show that the plume is coming from the direction of the Montour power plant in central PA. The second plume, due to transport from the Midwestern USA, was encountered on 22 July at 700–1500 m altitude above the RV Ron Brown which was sampling in the Gulf of Maine. On both occasions, the AMS data, processed with a constant CE of 0.5, had a peak SO_4^{2-} concentration above 50 μg m^{-3}, a coincident organic peak not associated with excess CO or light absorption, and a very nonlinear relation between aerosol volume derived from the AMS and PCASP. Figure 7 shows the AMS-PCASP volume relation with a constant CE = 0.5 and with a CE which varies between 0.5 and 1 based on acidity according to equation (2). The low concentration points are outside of the SO_4^{2-} plume and because the NH_4^+ to SO_4^{2-} ratio is greater than 1, equation (2) gives CE = 0.5; that is, the acidity dependence of CE has no effect on AMS results. Data points within the acidic SO_4^{2-} plume have higher concentrations and volumes. Graphically, these points appear to be above the trend line established by the low concentration points. AMS volumes calculated with equation (2) yield a lower volume so that the entire data set more nearly follows a single trend line. This was the basis for constructing equation (2). It is only partially successful, as there are still some data points that are scattered above the trend line. Equation (2), however, does get rid of the very high concentration peaks which yield AMS/PCASP volume ratios almost two times higher than the campaign median. In constructing equation (2) we have relied on the experience of several research groups who have found that a CE of 0.5 yields good agreement between the AMS and filter or PILS samples. We account

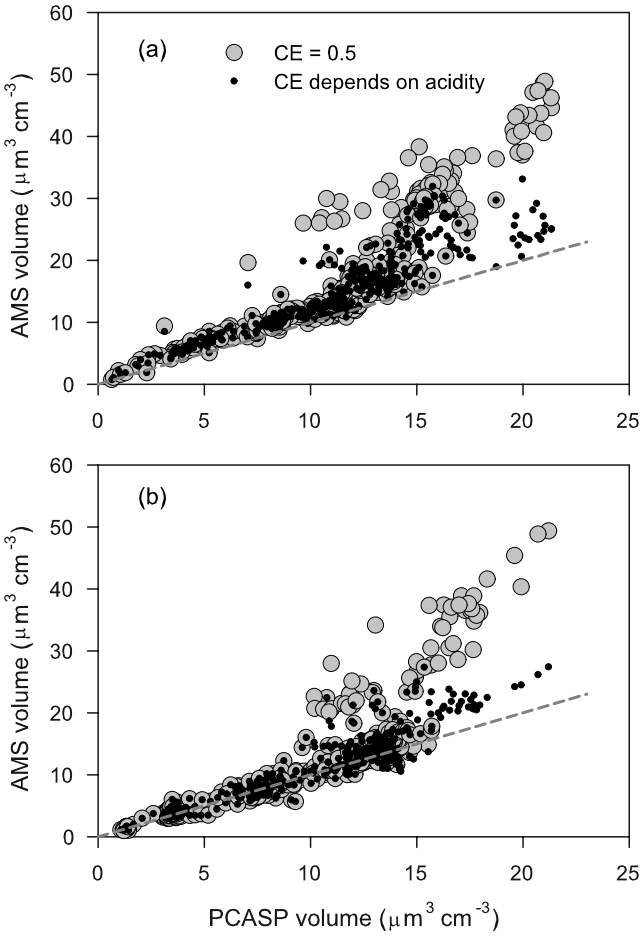

Figure 7. Comparison of accumulation mode aerosol volume determined from the AMS and PCASP (including sub 100 nm contribution from the DMA) for (a) 21 July and (b) 22 July. The figures show AMS data with a constant CE of 0.5 and with an acid dependent CE given by equation (2). Dashed lines are 1 to 1.

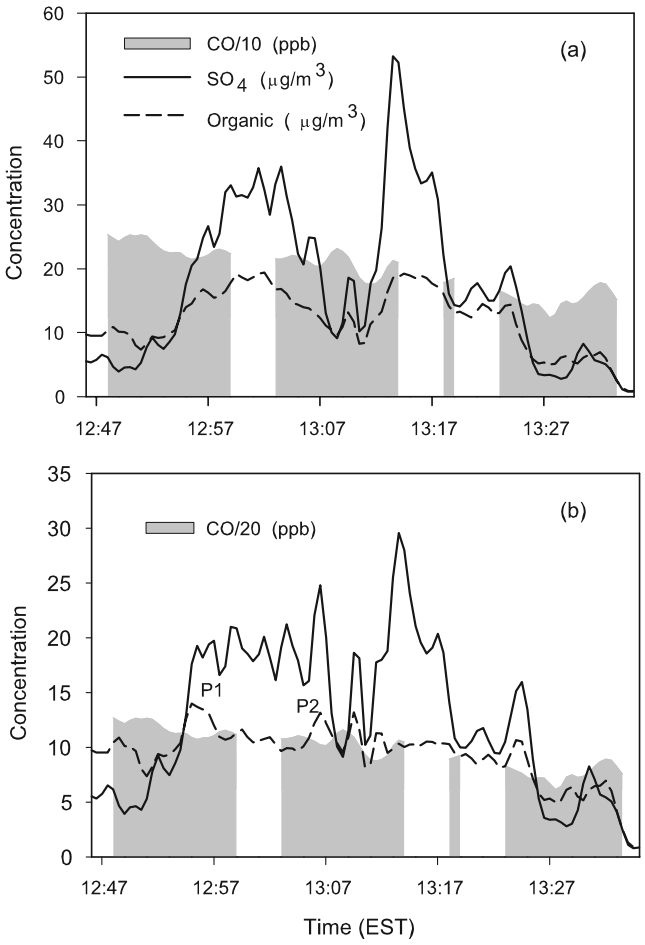

Figure 8. Time series of SO_4^{2-}, organic aerosol, and CO during the 22 July flight. Missing CO data are due to instrument zeroes. (a) Aerosol concentration determined with a constant CE = 0.5. (b) Aerosol concentration determined with a variable CE given by equation (2). Organic peaks P1 and P2 are likely artifacts of an imperfect CE correction procedure. Data points from these peaks are among the points in Figure 7b which still have a high AMS/PCASP volume ratio after the acid-dependent CE correction has been applied. CO concentrations are the same in both panels.

for the acidity dependence of CE, but as can be seen in Figures 5 and 7 or Table 4, equation (2) does not constitute an AMS normalization designed to yield a 1 to 1 relation with PCASP or DMA volumes.

[38] Figure 8a shows that with a constant CE equal to 0.5, the high SO_4^{2-} plumes on 22 July are accompanied by a coincident increase in organic aerosol. These organic plumes are not associated with CO or light absorption making it unlikely that they are due to urban emissions which coincidentally overlap the SO_4^{2-} plumes. This is a potentially exciting result as laboratory experiments indicate that there is enhanced production of organics in acidic aerosols [*Jang et al.*, 2002]. However, upon correcting the data for the dependence of CE on acidity, the organic peaks mostly disappear (Figure 8b). These results demonstrate the difficulty in affirming the presence or absence of acid-catalyzed organic aerosol production in cases where CE depends on acidity.

6. Aerosol Composition and Size Spectra

[39] The reader is referred to Figures 1 and 2 which show aircraft flight tracks and an aerosol concentration time series. Composition data are summarized in Table 1 and Figure 9. On most days aerosol composition is dominated by the organic component. Exceptions are confined mainly to four flights on 14, 21, and 22 July and 5 August in which aerosol concentrations up to 60 $\mu g\ m^{-3}$ were observed by the AMS. For these high concentration periods, organic aerosols are about 10–20 $\mu g\ m^{-3}$ with most of the remainder being SO_4^{2-} and associated NH_4^+. Nitrate concentrations rarely exceeded 1 $\mu g\ m^{-3}$ and Cl^- was below 0.1 $\mu g\ m^{-3}$. The bar graph in Figure 9 illustrates a shift from an organic dominated aerosol at low concentration to an aerosol that is one-half SO_4^{2-} at high concentration. The organic fraction decreases with total concentration from 73% when the total aerosol mass is less than 10 $\mu g\ m^{-3}$ to 41% in the highest concentration subset (>30 $\mu g\ m^{-3}$). Measurements made during the same time period aboard the RV Ron Brown likewise show that the submicron aerosol contains a high fraction of organic material: 68% of a total of 11 $\mu g\ m^{-3}$ for NW flow and 41% for more polluted SW flow with an average total concentration of 30 $\mu g\ m^{-3}$ [*Bates et al.*, 2005]. These percentages, as a function of aerosol loading, are almost identical to our aircraft observations which suggests that the Ron Brown observations may be representative of a larger area than coastal New England.

[40] Although *Bates et al.* [2005] found reasonable agreement between their measurements on the Ron Brown and those from near-by IMPROVE sites, the IMPROVE network in general indicates an aerosol composition with more SO_4^{2-} and less organics. In an analysis of 2002 data for the Northeastern USA, *Malm et al.* [2004] report an average July–August $PM_{2.5}$ concentration of about 8 $\mu g\ m^{-3}$, consisting of approximately 60% NH_4^+–SO_4^{2-}, 28% organic, 2% NO_3^-, and 10% EC and crustal material. The proportion

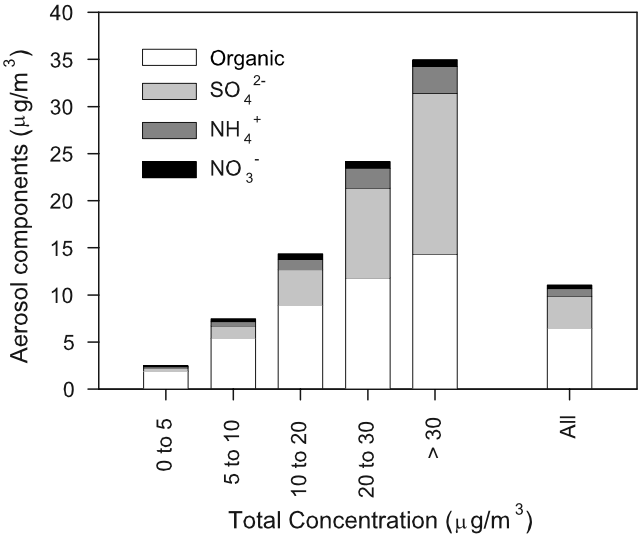

Figure 9. Average aerosol composition from AMS measurements presented as a function of total concentration.

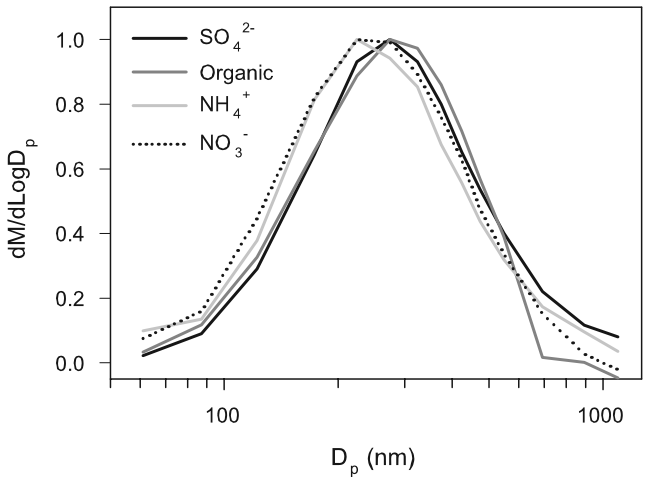

Figure 10. Average AMS size spectra for SO_4^{2-}, organics, NH_4^+, and NO_3^-. Spectra are normalized to have a peak value of 1.

of SO_4^{2-} is known to increase in pollution episodes with the worst visibility [*Northeast States for Coordinated Air Use Management*, 2001].

[41] Figure 10, which presents the average AMS size distributions for SO_4^{2-}, organics, NH_4^+, and NO_3^-, all normalized to have a peak value of 1, supports the picture that to a first approximation aerosol constituents are internally mixed. Aside from a small shift to a smaller size for NH_4^+, and NO_3^-, the normalized dM/dlogD_ps are almost identical. Although the size distributions averaged over the whole campaign are similar, there are time periods where the size distributions differ.

7. Secondary Aerosol Production and Aerosol Light Absorption

[42] Production of secondary organic aerosol and changes in aerosol light absorption have been quantified by examining the ratios of organic aerosol and light absorption to the conservative tracer, CO, as a function of photochemical age. Ideally, this type of experiment is carried out under conditions where a source region with known properties can be identified. Samples taken at varying downwind distances are then analyzed to yield a kinetic description of how composition or other properties change with atmospheric residence time or exposure to an atmospheric oxidant such as OH. *Brock et al.* [2005] have examined the formation of soluble organic aerosol downwind of major urban areas in the Eastern USA. *Takegawa et al.* [2006] have followed changes in SOA as a function of photochemical age at a fixed site downwind of Tokyo. *Volkamer et al.* [2006] use time of day as yardstick to gauge SOA production.

[43] Our sampling methodology in this study necessitates a different approach. Instead of identifying data from a discrete source, we use data with high CO concentration (>150 ppb). For the most part, high CO air masses result from urban emissions, which will also be a source of NO_x, POA, and SOA precursors. However, because of the abundance of emission sources in our sampling domain, high CO samples will contain a mixture of pollutants with varying atmospheric residence times. There will be cases where the organic aerosol, light absorbing BC, inert tracer, and photochemical age species are coming from different sources. Thus, we expect a great deal of scatter in the ratio of organic aerosol or light absorption to CO as a function of photochemical age. These same tracer ratios can be determined from measurements at surface sites in high emission rate regions, under conditions where it is logical to assume that the organic aerosol is nearly all primary and that the optical properties of BC are minimally affected by atmospheric processing. By comparing our measurements with surface ratios, we obtain an estimate of the fraction of organic aerosol that is secondary [*Turpin and Huntzicker*, 1995] and an estimate of changes in light absorption due to atmospheric processing.

7.1. Photochemical Age

[44] As a measure of chemical processing in the atmosphere we have used the ratio NO_x/NO_y which has an initial value of one at a NO_x emission source. Oxidation of NO_2 to products such as HNO_3, organic nitrates, and PAN causes the ratio NO_x/NO_y to decrease. During daytime hours most of the oxidation of NO_x is due to reaction with OH radical, and therefore the age ratio is related to the time integrated exposure of an air mass to OH radical according to

$$\log(NO_x/NO_y) = k[OH]t \quad (4)$$

where k is the rate constant for NO_2 + OH, [OH] is a time averaged OH concentration, and t is time. The product of [OH] and t is referred to as photochemical age and is a useful metric of atmospheric processing. There is an extensive literature on the use hydrocarbon ratios to determine photochemical age and atmospheric residence times, which applies also to NO_x/NO_y [e.g., *Parrish et al.*, 1992; *Kleinman et al.*, 2003]. Problems derive from the fact that emission sources are spatially distributed so there is not a single well-defined atmospheric residence time. The exponential relation between NO_x/NO_y and k[OH]t can then cause a nearby small source to have a greater influence on photochemical age than a large distant source. As a result, the photochemical age method underestimates the exposure of pollutants in an air mass to OH, with the underestimate becoming larger for aged samples. We also note that our analysis includes samples that spent all or part of their atmospheric residence during the night where $O_3 + NO_2$ is the major mechanism for removing NO_x. While NO_x/NO_y may not yield quantitative information on photochemical age, it is qualitatively useful even in areas with multiple emission sources in that lower ratios generally indicate a more aged air mass [*Olszyna et al.*, 1994].

7.2. Data Set and Method

[45] Our conservative tracer is CO which is slowly oxidized in the atmosphere, but over the timescales of interest here (hours to possibly days), may be regarded as inert. Black carbon is chemically inert but can be removed by wet deposition if it is internally mixed with soluble aerosol constituents [*Park et al.*, 2005a]. Under our fair weather sampling conditions, wet deposition can be ignored and BC should, to an excellent approximation, be conserved. Aerosol light absorption, in contrast, is expected to change as

an aerosol ages [*Chýlek et al.*, 1995; *Jacobson*, 2001]. We have also examined the ratio of organics at mass peak 44 (M44) to total organic concentration as an indicator of atmospheric processing.

[46] The age analysis is based on 20% of the total data set with CO > 150 ppb and concurrent measurements of organic aerosol, NO_x, NO_y, and light absorption. Median CO in this data subset is 190 ppb. Four flights are not represented: 17 July because of missing PSAP data and 10 July and 7 August (two flights) because of low CO. The resulting data set contained periods with high and rapidly changing SO_2 indicating passage though nearby utility plumes. Utility plume transects which had significantly elevated NO_x relative to adjacent nonplume air were not included in the age analysis. These points, accounting for 1.6% of the total data set, have a low photochemical age that is not related to the processing of urban aerosols. Most of the omitted plume points are from the 16 July flight which was designed to sample downwind of an industrial-utility complex near the DE-PA border (see Figure 1 and *Kleinman et al.* [2004]). Utility plumes without excess NO_x were left in the age calculations. Without NO_x there is no perturbation to photochemical age and it is a simple consequence of the congestion of emission sources in the Northeastern USA that air masses will contain a mixture of urban and utility emissions. The resulting data will be referred to as the "CO-plume" data subset.

[47] Background values were subtracted for CO, organic aerosol, M44, and light absorption because we are interested in examining perturbations due to local and regional emission sources. Background CO was determined as the median value of CO concentration when the organic aerosol concentration was near zero. This yielded a CO concentration of 90 ppb. Backgrounds for other quantities were evaluated as median values over a data subset with CO between 80 and 100 ppb. The resulting backgrounds were organic aerosol concentration = 1.3 $\mu g\ m^{-3}$, M44 = 0.15 $\mu g\ m^{-3}$, and light absorption = 0.8 Mm^{-1}. Sensitivity studies were done for cleaner and more polluted backgrounds, representing in a qualitative way uncertainties in these values. Quantities in which a background has been subtracted will be denoted by a "Δ". Background correction can be problematic because the single background composition that we are using will not be an appropriate upwind condition for all polluted air masses. Fortunately, in most cases, signals are severalfold greater than the background. There are, however, cases where background and signal are comparable. This leads to a subset of points with either very low or very high ratios according to whether the Δ quantity is in the numerator or denominator.

[48] Data trends are given by a locally weighted regression scatterplot smoothing (Lowess) calculation which yields a locally linear but globally nonlinear regression fit [*Cleveland and Devlin*, 1988]. This procedure does not yield error estimates, so in three cases where quantitative information is desired, figures include a linear least squares regression line with 95% confidence intervals.

[49] Eighty-two percent of our data set is from daytime flights. It was not possible to differentiate between the effects of daytime and nighttime chemical processing because pollutants measured at night could have been emitted during the day and vice versa. Part of our data set is from transects through discrete urban plumes at varying downwind distances and part is from regional pollution events with low values of NO_x/NO_y. Despite the dilution that accompanies aging, the aged air masses actually have a higher median CO concentration than the near-source samples. On the basis of trajectories and transport distances, at least some of the samples with the lowest NO_x/NO_y ratios (<0.1) have transport times greater than 24 h. As a category, the aged air masses also had SO_4^{2-} concentrations severalfold greater than the younger high NO_x/NO_y samples, consistent with a long atmospheric residence time.

[50] NO_x/NO_y ratios range from 0.8 to 0.05 but only 3% of the data points have a NO_x/NO_y ratio above 0.5. To some extent this is a result of our sampling protocol which did not emphasize sampling near large emission sources. In previous midboundary layer altitude flights in Phoenix and Philadelphia we have found that the median values for NO_x/NO_y near the urban centers ranged from 0.50 for Phoenix in the morning to 0.16 for Philadelphia in the afternoon [*Kleinman et al.*, 2005]. It has been our experience in these and other cities that samples taken over urban downtown areas can have atmospheric residence times of a few hours reflecting the fact that air at 300–500 m altitude contains pollutants from a multikilometer size footprint.

[51] Surface observations have been used to determine the ratio of organic aerosol to tracer that is characteristic of fresh emissions. The surface value of ΔOrganic/ΔCO is based on the work of *Chen et al.* [2001] who measured CO and EC at a suburban site in the Baltimore-Washington corridor. To convert EC to organic mass, we use a value of 2 for the OC/EC ratio [*Turpin and Huntzicker*, 1995; *Park et al.*, 2005b]. The latter study cites a range of primary OC/EC ratios of 1.5 to 2.4 from the literature and a range of 1.7 to 3 for Baltimore. A value of 1.6 was used for the ratio of organic mass to organic carbon, OA/OC, following the recommendation of 1.6 ± 0.2 from *Turpin and Lim* [2001]. *Chen et al.* [2001] found that the EC/CO ratio varied with time of the year and temperature. We used a value of 6.7×10^{-3} ($\mu g\ m^{-3}$ EC/$\mu g\ m^{-3}$ CO) for the summer season and high temperatures that match our experimental conditions. Other authors have reported EC/CO ratios 50% to as much as a factor of 5 lower [*Baumgardner et al.*, 2002; *Park et al.*, 2005b]. On the basis of the above observations, a surface value of ΔOrganic/ΔCO = 0.02 $\mu g\ m^{-3}$/ppb results from:

$$\Delta\text{Organic}/\Delta\text{CO} = \left(0.95\ \mu\text{gm}^{-3}\ \text{CO/ppb CO}\right) \times (\text{EC/CO}) \times (\text{OC/EC}) \times (\text{OA/OC}), \quad (5)$$

As the surface ratio representative of fresh emissions is (POA/CO) and the aircraft ratio is ((SOA + POA)/CO), the percent SOA in the aircraft sample is given by:

$$\%\ \text{SOA} = 100 \times \left(1 - (\Delta\text{Organic}/\Delta\text{CO})_{\text{Surface}}/(\Delta\text{Organic}/\Delta\text{CO})_{\text{G1}}\right) \quad (6)$$

A surface value for ΔAbsorption/ΔCO is estimated based on the EC/CO ratio mentioned above. In addition, we need to know the response of the PSAP to EC which is described

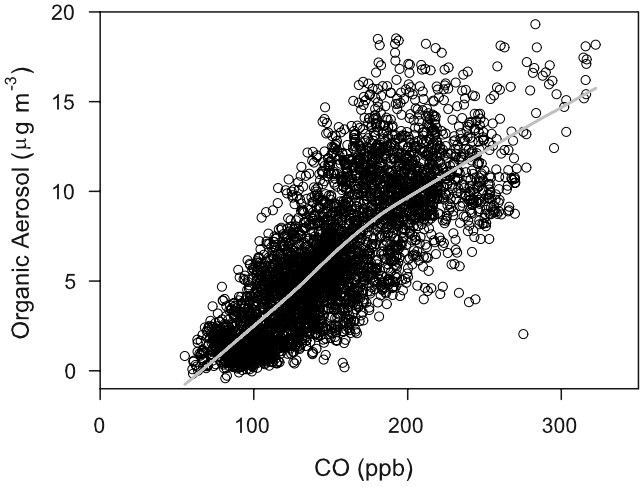

Figure 11. Organic aerosol versus CO for the entire data set. Solid line is a Lowess fit.

by the parameter σ (mass absorption efficiency) determined from concurrent measurements of light absorption and EC:

$$\text{PSAP light absorption} = \sigma\ \text{EC} \tag{7}$$

Depending on location and conditions, σ has been found to vary from 5 to 20 $m^2\ g^{-1}$ [*Liousse et al.*, 1993]. *Schuster et al.* [2005] have studied the effects of atmospheric processing on aerosol light absorption using calculated and measured values of σ for AERONET climatologies. AERONET retrievals indicate an average value for σ of 9.9 $m^2\ g^{-1}$, equal to the geometric midpoint from *Liousse et al.* [1993]. The calculated σ for an external mixture of fine mode BC is 4.3 $m^2\ g^{-1}$, the enhanced absorption in the climatological average being ascribed to the creation of internal mixtures. We will compare these values of σ with that calculated from our data set using:

$$\sigma = (\Delta\text{Absorption}/\Delta\text{CO}) \Big/ \left[\left(0.95\ \mu\text{gm}^{-3}\text{CO/ppb CO}\right) \times (\text{EC/CO})\right] \tag{8}$$

7.3. Results

[52] Figure 11 shows the relation between organic aerosol measured with the AMS and concurrently measured CO. There is a clear tendency for high CO air masses to have high concentrations of organic aerosol. As previously discussed, there are several reasons for scatter. First, there is measurement uncertainty estimated to be about 5% for CO and approximately 35% for a single 30-s AMS measurement (see AMS/PCASP entry in Table 4). Second, background values of CO and organic aerosol vary. The low CO data points in Figure 11 suggest a background CO and organic variability of around 10 ppb and 1 $\mu g\ m^{-3}$, respectively. Third, sources in our sampling domain emit CO and organic aerosol in varying proportions. Literature references are given in section 7.2. Fourth, and of most interest, are systematic changes to organic aerosols due to atmospheric processing. Factors 1 to 3 are essentially random, so that trends in the organic to CO ratio can be interpreted in terms of atmospheric processing. Similar considerations apply to the relation between aerosol light absorption and CO.

[53] In Figure 12 we focus on the "CO-plume" data subset. Those points which represent air masses that contain relatively fresh emissions, as indicated by a NO_x to NO_y ratio above 40%, are seen to have low values of organic aerosol and light absorption for a given CO concentrations. That is, most of these points lie below the Lowess fit to the entire CO-plume data subset. Note that this result is independent of assumptions on background.

7.4. Aerosol Ageing

[54] Aerosol ageing is examined in Figures 13 and 14 by using CO as a conservative tracer of urban emissions and plotting ΔOrganic/ΔCO and ΔAbsorption/ΔCO versus $-\log(NO_x/NO_y)$. As plotted, age increases from left to right.

[55] A diamond on the right side of Figure 13 indicates the organic aerosol to CO ratio deduced from the surface observations presented above, under conditions where the aerosol is nearly all primary, emitted material. An extension of the Lowess fit to zero photochemical age yields an

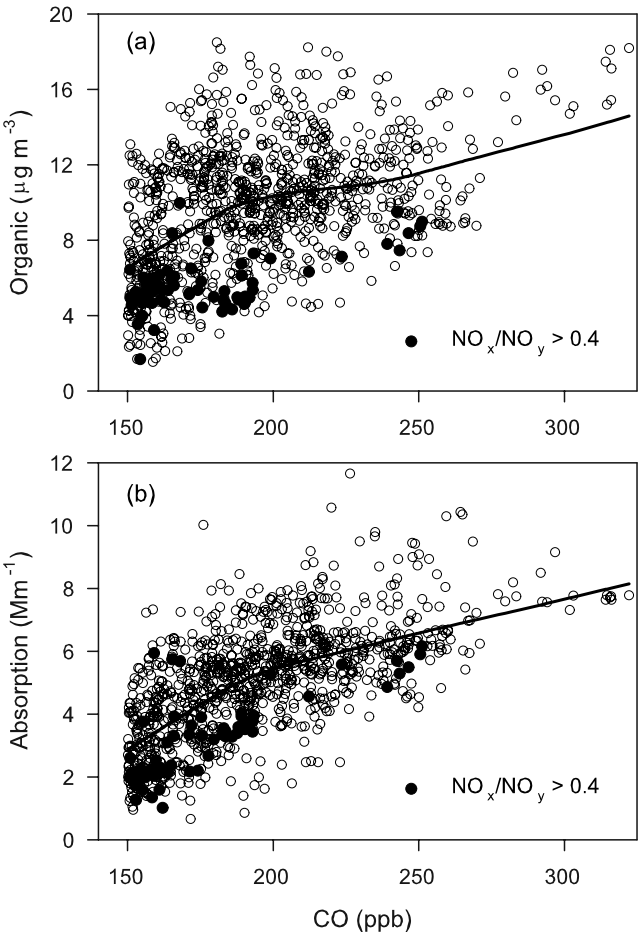

Figure 12. Organic aerosol and aerosol light absorption versus CO in panels (a) and (b), respectively, for CO-plume data subset, defined in section 7.2. Data points are sparser than in Figure 11 because of the requirement for simultaneous measurements of organic aerosol, light absorption, NO_x, NO_y, and CO > 150 ppb. Solid lines are Lowess fits. Solid circles have NO_x > 40% of NO_y.

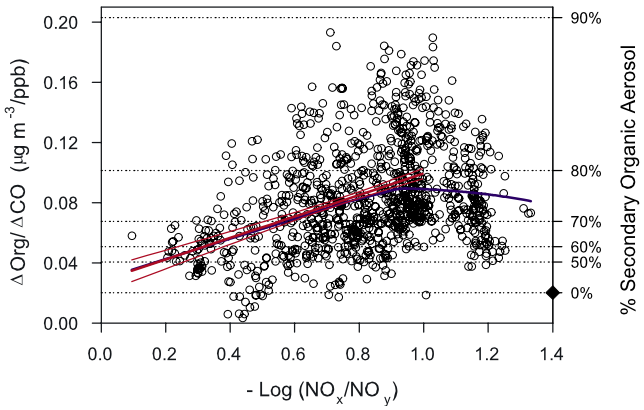

Figure 13. ΔOrganic/ΔCO as a function of atmospheric ageing given by $-\log(NO_x/NO_y)$ for CO-plume data subset. Diamond on right hand axis gives an inferred surface ratio of ΔOrganic/ΔCO from equation (5) under conditions where the organic aerosol is mainly primary. On the basis of this ratio, the right-side scale calculated from equation (6) gives the correspondence between observed ΔOrganic/ΔCO and the percentage of organic aerosol that is secondary. Blue line is a Lowess fit. Red lines are a linear least squares regression fit to data with 95% confidence intervals. Regression uses data with $-\log(NO_x/NO_y) < 1$.

intercept at about 30% SOA. This could represent rapid SOA production in the near source region, but the 95% confidence limit on the regression includes 0% SOA, so this result has limited statistical significance. For most of the data set, the organic aerosol to CO ratio is much larger than the near-source value, indicating that more than 70% of the organic aerosol is secondary. The Lowess fit shows that the amount of organic aerosol per CO increases fourfold between the fresh emission limit and the maximum which is reached when $NO_x/NO_y = 10\%$. The rate of increase of SOA is 40% of the apparent rate for the transformation of NO_x into NO_y. If, for example, it takes 1 day to reach $NO_x/NO_y = 10\%$, it implies that SOA is added to the air mass at an average rate of 6% h^{-1}. This rate could represent the SOA formation rate from VOCs that are coemitted with the CO tracer or alternately could be due to SOA production from downwind biogenic sources. Annual average data for $PM_{2.5}$ in our sampling region from the IMPROVE network [*Malm et al.*, 2004] (modified for an organic mass to organic C ratio of 1.6) yields a % SOA of about 75%. A similarly large fraction of SOA was found by *de Gouw et al.* [2005] in samples taken in the Gulf of Maine and off the East Coast of the USA, in a time period that overlapped our study. The source of the organic aerosol is problematic. On the basis of an analysis of VOC observations and published aerosol yields, *de Gouw et al.* [2005] found that anthropogenic compounds accounted for only 14% of SOA and that biogenic compounds made only a minor contribution.

[56] Figure 14 shows that aerosol light absorption ratioed to the conservative tracer CO, increases by a factor of 2.4 between the youngest and oldest air masses, as defined by the two ends of the Lowess fit to the plume-CO data set. As the mass of BC that is causing the light absorption should not change with photochemical age, this result implies that σ, the mass absorption efficiency, increases with age by the same factor of 2.4. This factor is similar to the increase implied by a comparison of global average AERONET absorptions (σ = 9.9 m^2 g^{-1}) with that determined for freshly emitted BC (σ = 4.3 m^2 g^{-1}) [*Schuster et al.*, 2005]. On the right hand axis of Figure 14 are values of σ calculated from equation (8) using the same value of 6.7×10^{-3} (μg m^{-3} EC/μg m^{-3} CO) that was used to determine SOA production in Figure 13. The predicted values of σ (3.0 to 7.2) are lower than that obtained from the study of Schuster et al. Decreasing the EC/CO ratio to 4.7×10^{-3}, which is well within the range of observations, brings our inferred σs into agreement with the cited literature values.

[57] Relevant changes during ageing that could explain the 2.4-fold increase in σ include the buildup of SOA (Figure 13) and an even larger increase in SO_4^{2-} (not shown). Effects of these changes on light absorption depend on the details on how BC and other aerosol ingredients are mixed, but the magnitude of the increase in specific absorption with age is appropriate for the deposition of nonabsorbing secondary aerosol and its lensing effect [*Chýlek et al.*, 1995; *Jacobson*, 2000; *Schnaiter et al.*, 2005; *Schuster et al.*, 2005]. As deposition of secondary aerosol implies an increase in aerosol concentration, we have examined ΔAbsorption/ΔCO as a function of total aerosol loading in Figure 15. The 2.4-fold change in σ determined from Figure 14 is seen to be a nearly linear function of total aerosol concentrations between 2 and 20 μg m^{-3}.

[58] It is difficult to assign an uncertainty to the %SOA values and light absorption changes shown in Figures 13 and 14 because we have only qualitative estimates for the uncertainties of the variables upon which our results depend. In place of a full uncertainty analysis we have varied input parameters and recalculated the median value for %SOA and the increase in mass absorption efficiency. As before this increase is defined as change in the Lowess fit to ΔAbsorption/ΔCO from the youngest to oldest air mass. Results are shown in Table 6, along with footnotes indicating the reason for each variation. Except for one case in which the

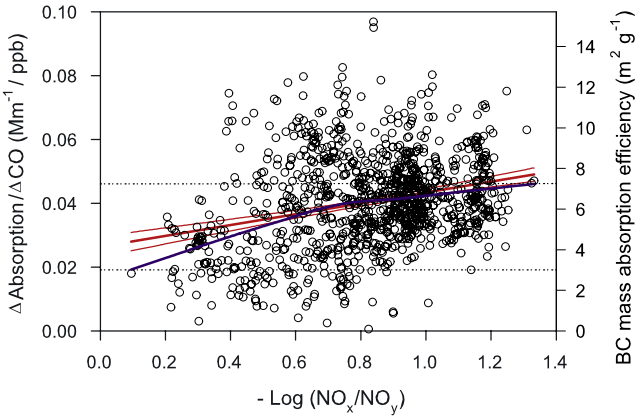

Figure 14. ΔAbsorption/ΔCO as a function of atmospheric ageing given by $-\log(NO_x/NO_y)$ for CO-plume data subset. Right-side axis is σ calculated from (9). Blue line is a Lowess fit. Dashed lines indicate range of σ (3.0 to 7.2) associated with the Lowess fit at minimum and maximum photochemical age. Red lines are a linear least squares regression fit with 95% confidence intervals.

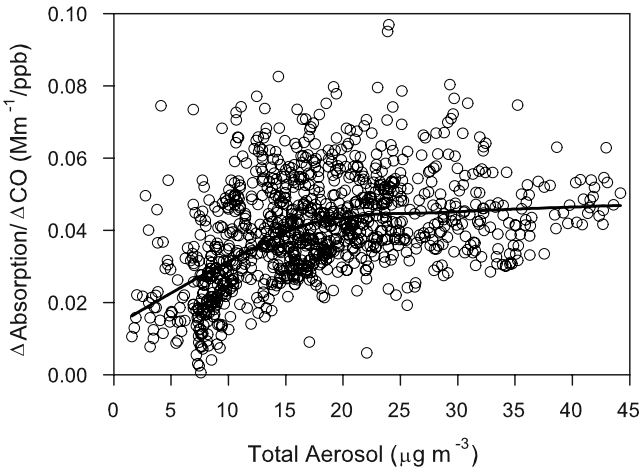

Figure 15. ΔAbsorption/ΔCO as a function of total aerosol concentration for CO-plume data subset. Solid line is a Lowess fit.

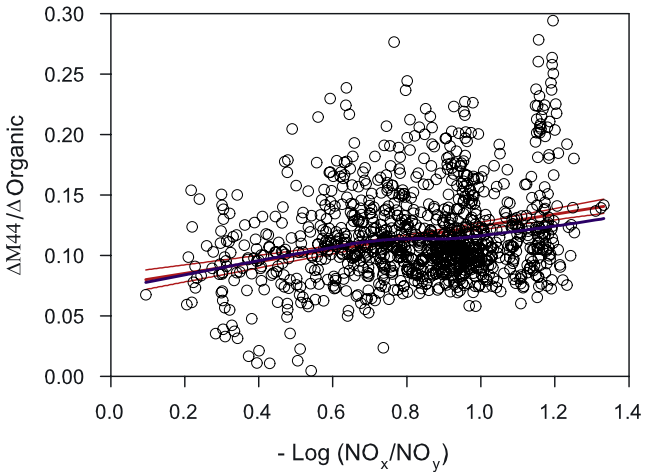

Figure 16. ΔM44/ΔOrganic as a function of atmospheric ageing given by $-\log(NO_x/NO_y)$ for CO-plume data subset. Blue line is a Lowess fit. Red lines are a linear least squares regression fit with 95% confidence intervals.

surface EC/CO ratio is doubled to what is probably an unrealistic value, the percentage of organic aerosol that is secondary is found to vary between 62 and 90%. The change in mass absorption efficiency is not dependent on any surface parameters but does show a ±20% sensitivity to background conditions.

[59] Figure 16 shows organic oxidation as measured by ΔM44/ΔOrganic as a function of photochemical age. Low photochemical age samples have a ΔM44/ΔOrganic ratio that is higher than the few percent value observed in unprocessed urban emissions [*Alfarra et al.*, 2004]. Over the observed range of photochemical ages, the Lowess fit indicates a steady increase in the organic oxidation surrogate from 0.08 to 0.13 (0.08 ± 0.01 to 0.14 ± 0.01 for the linear regression fit).

8. Conclusions

[60] The 2002 NEAQS campaign was the second field program in which the Aerodyne AMS was used for aircraft sampling. This was a demanding application for the AMS because the spatial inhomogeneity of emission sources in our sampling regions dictated a sampling frequency an order of magnitude faster than typically used. We have assessed the performance of the AMS by comparison with

Table 6. Sensitivity of SOA and Aerosol Light Absorption to Measurement Uncertainties

Parameter	Median % SOA from ΔOrganic/ΔCO	Light absorption increase over age range from ΔAbsorption/ΔCO[a]
Base case	74	2.4
Absorption increase from regression	Not applicable	1.8
AMS volume/1.46 to match PCASP[b]	62	Not applicable
Organic IE = 1.3 in place of 1.4[c]	76	Not applicable
Organic IE = 1.9 in place of 1.4[c]	65	Not applicable
Cleaner background[d]	73	2.8
More polluted background[e]	75	1.9
Surface EC/CO = 1/2 of 6.7×10^{-3}[f]	87	2.4
Surface EC/CO = $2 \times 6.7 \times 10^{-3}$[f]	48	2.4
OA at surface is only 50% primary[g]	87	Not applicable
OA/OC changed from 1.6 to 1.2[h]	81	Not applicable

[a]Light absorption increase from Lowess curve, except as noted.

[b]The maximum change in AMS volume consistent with other observations, is obtained by dividing by 1.46 to match the PCASP volume. Changing the AMS volume to match DMA volume or observed light scattering results in a decrease in organic concentration of a factor of 1.25 and 1.18, respectively. See Tables 4 and 5.

[c]Laboratory experiments on different organic aerosols place the ionization efficiency, relative to NO_3^-, between 1.3 and 1.9. See section 3.

[d]Background CO = 70 ppb, organic aerosol = 0 μg m^{-3}, and light absorption = 0 Mm^{-1}.

[e]Background from samples with CO between 80 and 120 ppb. CO = 103 ppb, organic aerosol = 2.1 μg m^{-3}, and light absorption = 1.2 Mm^{-1}.

[f]Effect is to change the surface ΔPOA/ΔCO ratio by a factor of 2. As described in section 7.2, there are observations in which the surface EC/CO ratio is a factor of 2 or more lower than the value used here. Because 6.7×10^{-3} is near the top of the range of observed values, a doubling is less realistic.

[g]Equivalent to decreasing surface ΔPOA/ΔCO ratio by a factor of 2.

[h]Lower value for OA/OC is appropriate for "hydrocarbon-like" organic aerosol, which can constitute a significant fraction of primary emissions [*Zhang et al.*, 2005b].

other aerosol instrumentation, namely a PCASP, DMA, and an integrating nephelometer. Results pertinent to the abundance of organic aerosol, the fraction of SOA, and the rate of formation of SOA are reported.

[61] In a 30-s sampling period with three point smoothing, the 1σ noise within the AMS during measurements in clean air was 0.09, 0.14, 0.05, 0.6, and 0.6 μg m^{-3} for SO_4^{2-}, NH_4^+, NO_3^-, organics, and total aerosol, respectively. The average aerosol concentration measured by the AMS was 11 μg m^{-3}. Only 6% of samples had a total concentrations lower than 1.3 μg m^{-3}, twice the clean-air noise level.

[62] Instrument intercomparisons were conducted for volume and for total light scattering at 550 nm. Comparisons were carried out over a subset of the accumulation mode (100–500 nm) in order to insure a common size range for the AMS, DMA, and PCASP; and for the full accumulation mode ending at 1000 or 1200 nm. Data from the DMA were considered with and without an extrapolation to cover the 500- to 1000-nm size range.

[63] Our overall assessment of the several ways of comparing our four aerosol instruments starts with the observation that the comparison between the DMA (with an extrapolation to 1000 nm) and nephelometer has a near zero bias. The DMA is generally regarded as the more direct and accurate instrument for determining volume and the nephelometer is our only direct measure of scattering. Compared with these instruments, the AMS has a median bias in volume of +25% (33% with an estimated refractory component), and a median bias in light scattering of +18%. There is a wide range in the amount of scatter from one comparison to the next. At one extreme is the comparison between observed light scattering and that calculated from the PCASP with a linear regression r^2 of 0.98, presumably because these instruments both operate on the same light scattering principle. At the other extreme are comparisons which involve the AMS or DMA size distribution (i.e., scattering calculation or 100–500 nm AMS volume) as these are inherently noisy for a single measurement period.

[64] A comparison between AMS and PCASP volume in 2 high concentration SO_4^{2-} plumes gives clear evidence that the CE (collection efficiency) of the AMS can vary by about a factor of 2 depending on aerosol acidity. On the basis of this comparison a CE correction factor was derived and applied to all of the AMS measurements. Concurrent measurements of CO, organics, and light absorption illustrate the difficulty of identifying acid catalyzed organic aerosol formation when detection efficiency depends on chemical composition.

[65] The observed amount and fraction of organic aerosol was comparable to measurements made in the same time frame in the Gulf of Maine [*Bates et al.*, 2005] but was higher than expected based on monitoring data from the IMPROVE network [*Malm et al.*, 2004]. Out of an average aerosol concentration of 11.1 μg m^{-3}, 58% or 6.5 μg m^{-3} was organic. The fraction of aerosol that is organic changes from over 70% at low aerosol concentration to about 40% in high concentration SO_4^{2-} plumes. Our results indicate that the observed high organic fraction measured off the coast of New England apply to a larger geographic area.

[66] The ratio of organic aerosol concentration and aerosol light absorption to CO concentration was examined as a function of atmospheric processing, approximated by the photochemical age marker, NO_x/NO_y. Ratios were compared with literature values for freshly emitted pollutants. The observed organic/CO ratio in young air masses, within statistical uncertainty, overlaps that expected from surface observations. There is a fourfold increase in the organic/CO ratio in air masses with NO_x/NO_y = 10%, equivalent to SOA being 75% of total organic aerosol. Over the observed range of photochemical ages, the ratio of aerosol light absorption to CO increases by a factor of 2.4. As light absorption is due primarily to BC, which like CO is assumed to be conservative, this increase is interpreted as a 2.4-fold increase in light absorption per unit mass of BC. Such an increase in light absorption is expected as atmospheric processing tends to create internal mixtures in which BC becomes surrounded by an increasing amount of organics and SO_4^{2-} [*Chýlek et al.*, 1995; *Jacobson*, 2000; *Schnaiter et al.*, 2005; *Schuster et al.*, 2005]. *Jacobson* [2001] has calculated a significant increase in global radiative forcing due to an increase in aerosol light absorption caused by atmospheric processing.

[67] The NEAQS G-1 observations demonstrate the ability of the AMS in combination with other optical and chemical instrumentation to give information on the time evolution of aerosol light absorption and SOA production. By using NO_x/NO_y as a photochemical age clock we are able to see the broad features of absorption and SOA changes. To improve this picture, we need to make measurements at various distances downwind of discrete sources so that a sequence of well-defined atmospheric residence times can be specified.

[68] **Acknowledgments.** We thank chief pilot Bob Hannigan and the flight crew from PNNL for a job well done. We gratefully acknowledge the Atmospheric Chemistry Program within the Office of Biological and Environmental Research of DOE for supporting field and analysis activities and for providing the G-1 aircraft. We also thank James Allan for sharing his data analysis software tools which were used to extract the AMS data and the DOE SBIR program (DEFG02-00ER82939) which funded the development of the flight-ready AMS for deployment on the G-1 aircraft as well as the development of the aircraft two-stage diffuser inlet system. This research was performed under sponsorship of the US DOE under contracts DE-AC02-98CH10886.

References

Alfarra, M. R., et al. (2004), Characterization of urban and rural organic particulate in the Lower Fraser Valley using two Aerodyne aerosol mass spectrometers, *Atmos. Environ.*, *33*, 817–823.

Allan, J. D., J. L. Jimenez, P. I. Williams, M. R. Alfarra, K. N. Bower, J. T. Jayne, H. Coe, and D. R. Worsnop (2003a), Quantitative sampling using an Aerodyne aerosol mass spectrometer: 1. Techniques of data interpretation and error analysis, *J. Geophys. Res.*, *108*(D3), 4090, doi:10.1029/2002JD002358.

Allan, J. D., et al. (2003b), Quantitative sampling using an Aerodyne aerosol mass spectrometer: 2. Measurements of fine particulate composition in two UK cities, *J. Geophys. Res.*, *108*(D3), 4091, doi:10.1029/2002JD002359.

Allan, J. D., et al. (2004), Submicron aerosol composition at Trinidad Head, California, during ITCT 2K: Its relationship with gas phase volatile organic carbon and assessment of instrument performance, *J. Geophys. Res.*, *109*(D23), D23S24, doi:10.1029/2003JD004208.

Anderson, T. L., and J. A. Ogren (1998), Determining aerosol radiative properties using the TSI 3563 integrating nephelometer, *Aerosol Sci. Technol.*, *29*, 57–69.

Bahreini, R., J. L. Jimenez, J. Wang, R. C. Flagan, J. H. Seinfeld, J. T. Jayne, and D. R. Worsnop (2003), Aircraft-based aerosol size and composition measurements during ACE-Asia using an Aerodyne aerosol mass spectrometer, *J. Geophys. Res.*, *108*(D23), 8645, doi:10.1029/2002JD003226.

Bates, T. S., P. K. Quinn, D. J. Coffman, J. E. Johnson, and A. M. Middlebrook (2005), Dominance of organic aerosols in the marine boundary layer over the Gulf of Maine during NEAQS 2002 and their

role in aerosol light scattering, *J. Geophys. Res.*, *110*, D18202, doi:10.1029/2005JD005797.

Baumgardner, D., G. Raga, P. I. Rosas, T. Castro, T. Kuhlbusch, A. John, and A. Petzold (2002), Diagnosing black carbon trends in large urban areas using carbon monoxide measurements, *J. Geophys. Res.*, *107*(D21), 8342, doi:10.1029/2001JD000626.

Bond, C. M., T. L. Anderson, and D. Campbell (1999), Calibration and intercomparison of filter-based measurements of visible light absorption by aerosols, *Aerosol Sci. Technol.*, *30*, 582–600.

Brechtel, F. J. (2003), Description and Assessment of a New Aerosol Inlet for the DOE G-1 Research Aircraft, Final Technical Report of work performed by BMI under contract #0000058843 to Brookhaven National Laboratory, Aug. 2003.

Brock, C. A., et al. (2003), Particle growth in urban and industrial plumes in Texas, *J. Geophys. Res.*, *108*(D3), 4111, doi:10.1029/2002JD002746.

Brock, C. A., A. G. Wollny, J. deGouw, C. Warneke, J. Holloway, A. M. Middlebrook, D. M. Murphy, J. A. Neuman, P. Peltier, and R. J. Weber (2005), Transport and evolution of aerosol plumes from urban and industrial sources in the Eastern U.S., Abstract A11E-06, AGU, Washington, D.C.

Buzorius, G., C. S. McNaughton, A. D. Clarke, D. S. Covert, B. Blomquist, K. Nielsen, and F. J. Brechtel (2004), Secondary aerosol formation in continental outflow conditions during ACE-Asia, *J. Geophys. Res.*, *109*, D24203, doi:10.1029/2004JD004749.

Chen, L.-W., B. G. Doddridge, R. G. Dickerson, J. C. Chow, P. K. Mueller, and W. A. Butler (2001), Seasonal variations in elemental carbon aerosol, carbon monoxide and sulfur dioxide: Implications for sources, *Geophys. Res. Lett.*, *28*, 1711–1714.

Chýlek, P., G. Videen, D. Ngo, R. G. Pinnick, and J. D. Klett (1995), Effect of black carbon on the optical properties and climate forcing of sulfate aerosols, *J. Geophys. Res.*, *100*, 16,325–16,332.

Cleveland, W. S., and W. S. Devlin (1988), Locally weighted regression: An approach to regression analysis by local fitting, *J. Am. Stat. Assoc.*, *83*, 596–610.

Collins, D. R., R. C. Flagan, and J. H. Seinfeld (2002), Improved inversion of scanning DMA data, *Aerosol Sci. Technol.*, *36*(1), 1–9.

DeCarlo, P., J. G. Slowik, D. R. Worsnop, P. Davidovits, and J. L. Jimenez (2004), Particle morphology and density characterization by combined mobility and aerodynamic diameter measurements: Part 1. Theory, *Aerosol Sci. Technol.*, *38*, 1185–1205, doi:10.1080/027868290903907.

de Gouw, J. A., et al. (2005), Budget of organic carbon in a polluted atmosphere: Results from the New England Air Quality Study in 2002, *J. Geophys. Res.*, *110*, D16305, doi:10.1029/2004JD005623.

Drewnick, F., J. J. Schwab, O. Hogrefe, S. Peters, L. Husain, D. Diamond, R. Weber, and K. L. Demerjian (2003), Intercomparison and evaluation of four semi-continuous $PM_{2.5}$ sulfate instruments, *Atmos. Environ.*, *37*, 3335–3350.

Drewnick, F., J. J. Schwab, J. T. Jayne, M. Canagaratna, D. R. Worsnop, and K. L. Demerjian (2004), Measurements of ambient aerosol composition during the PMTACS-NY 2001 using an Aerosol Mass Spectrometer: Part I. Mass concentrations, *Aerosol Sci. Technol.*, *38*(S1), 92–103.

Griffin, R. J., D. Dabdub, M. J. Kleeman, M. P. Fraser, G. R. Cass, and J. H. Seinfeld (2002), Secondary organic aerosol: 3. Urban/regional scale model of size- and composition-resolved aerosols, *J. Geophys. Res.*, *107*(D17), 4334, doi:10.1029/2001JD000544.

Haller, A. G., et al. (2006), Atmospheric radiation measurements aerosol intensive operating period: Comparison of aerosol scattering during coordinated flights, *J. Geophys. Res.*, *111*, D05S09, doi:10.1029/2005JD006250.

Jacobson, M. Z. (2000), A physically-based treatment of elemental carbon optics: Implications for global direct forcing of aerosols, *Geophys. Res. Lett.*, *27*, 217–220.

Jacobson, M. Z. (2001), Strong radiative heating due to the mixing state of black carbon in atmospheric aerosols, *Nature*, *409*, 695–697.

Jang, M., N. M. Czoschke, S. Lee, and R. M. Kamens (2002), Heterogeneous atmospheric aerosol production by acid-catalyzed particle-phase reactions, *Science*, *298*, 814–817.

Jayne, J. T., D. C. Leard, X. Zhang, P. Davidovits, K. A. Smith, C. E. Kolb, and D. R. Worsnop (2000), Development of an aerosol mass spectrometer for size and composition analysis of submicron particles, *Aerosol Sci. Technol.*, *33*, 49–70.

Jimenez, J. L., et al. (2003), Ambient aerosol sampling using the Aerodyne aerosol mass spectrometer, *J. Geophys. Res.*, *108*(D7), 8425, doi:10.1029/2001JD001213.

Kleinman, L. I., et al. (2003), Photochemical age determinations in the Phoenix metropolitan area, *J. Geophys. Res.*, *108*(D3), 4096, doi:10.1029/2002JD002621.

Kleinman, L. I., W. F. Ryan, P. H. Daum, S. R. Springston, Y.-N. Lee, L. J. Nunnermacker, and J. Weinstein-Lloyd (2004), An ozone episode in the Philadelphia metropolitan area, *J. Geophys. Res.*, *109*(D20), D20302, doi:10.1029/2004JD004563.

Kleinman, L. I., P. H. Daum, Y.-N. Lee, L. J. Nunnermacker, S. R. Springston, J. Weinstein-Lloyd, and J. Rudolph (2005), A comparative study of ozone production in 5 U.S. metropolitan areas, *J. Geophys. Res.*, *110*, D02301, doi:10.1029/2004JD005096.

Leaitch, W. R., and G. A. Isaac (1991), Tropospheric aerosol size distributions from 1982 to 1988 over Eastern North America, *Atmos. Environ.*, *25a*, 601–619.

Liousse, C., H. Cachier, and S. G. Jennings (1993), Optical and thermal measurements of black carbon aerosol content in different environments: Variation of the specific attenuation cross-section, sigma (σ), *Atmos. Environ.*, *27a*, 1203–1211.

Liu, Y., and P. H. Daum (2000), The effect of refractive index on size distributions and light scattering coefficients derived from optical particle counters, *J. Aerosol Sci.*, *8*, 945–957.

Malm, W. C., B. A. Schichtel, M. L. Pitchford, L. L. Ashbaugh, and R. A. Eldred (2004), Spatial and monthly trends in speciated fine particle concentration in the United States, *J. Geophys. Res.*, *109*, D03306, doi:10.1029/2003JD003739.

Moore, K. G., II, et al. (2004), A comparison of similar aerosol measurements made on the NASA P3-B, DC-8, and NSF C-130 aircraft during TRACE-P and ACE-Asia, *J. Geophys. Res.*, *109*, D15S15, doi:10.1029/2003JD003543.

North American Research Strategy for Tropospheric Ozone (2003), *Particulate Matter Science for Policy Makers; A NARSTO Assessment,* EPRI 1007735.

Northeast States for Coordinated Air Use Management (2001), Regional Haze and Visibility in the Northeast and Mid-Atlantic States, Project Manager Gary Kleiman, Boston, MA, available at http://www.nescaum.org.

Olszyna, K. J., E. M. Bailey, R. Simonaitis, and J. F. Meagher (1994), O_3 and NO_y relationships at a rural site, *J. Geophys. Res.*, *99*, 14,557–14,563.

Park, R. J., et al. (2005a), Export efficiency of black carbon aerosol in continental outflow: Global implications, *J. Geophys. Res.*, *110*, D11205, doi:10.1029/2004JD005432.

Park, S. S., D. Harrison, J. P. Pancras, and J. M. Ondov (2005b), Highly time-resolved organic and elemental carbon measurement at the Baltimore Supersite in 2002, *J. Geophys. Res.*, *110*, D07S06, doi:10.1029/2004JD004610.

Parrish, D. D., C. J. Hahn, E. J. Williams, R. B. Norton, F. C. Fehsenfeld, H. B. Singh, J. D. Shetter, B. W. Gandrud, and B. A. Ridley (1992), Indications of photochemical histories of Pacific air masses from measurements of atmospheric trace species at Point Arena, California, *J. Geophys. Res.*, *97*, 15,883–15,901.

Quinn, P. K., D. J. Coffman, T. S. Bates, T. L. Miller, J. E. Johnson, E. J. Welton, C. Neusüss, M. Miller, and P. J. Sheridan (2002), Aerosol optical properties during INDOEX 1999: Means, variability, and controlling factors, *J. Geophys. Res.*, *107*(D19), 8020, doi:10.1029/2000JD000037.

Salcedo, D., et al. (2005), Characterization of ambient aerosols in Mexico City during the MCMA-2003 campaign with Aerosol Mass Spectrometry: Part 1. Quantification, shape related collection efficiency, and comparison with collocated instruments (2005), *Atmos. Chem. Phys. Disc.*, *5*, 4143–4182.

Schnaiter, M., C. Linke, O. Möhler, K.-H. Naumann, H. Saathoff, R. Wagner, U. Schurath, and B. Wehner (2005), Absorption amplification of black carbon internally mixed with secondary organic aerosol, *J. Geophys. Res.*, *110*, D19204, doi:10.1029/2005JD006046.

Schuster, G. L., O. Dubovik, B. N. Holben, and E. C. Clothiaux (2005), Inferring black carbon content and specific absorption from Aerosol Robotic Network (AERONET) aerosol retrievals, *J. Geophys. Res.*, *110*, D10S17, doi:10.1029/2004JD004548.

Slowik, J. G., K. Stainken, P. Davidovits, L. R. Williams, J. T. Jayne, C. E. Kolb, D. R. Worsnop, Y. Rudich, P. DeCarlo, and J. L. Jimenez (2004), Particle morphology and density characterization by combined mobility and aerodynamic diameter measurements: Part 2. Application to combustion generated soot particles as a function of fuel equivalence ratio, *Aerosol Sci. Technol.*, *38*, 1206–1222, doi:10.1080/027868290903916.

Springston, S. R., L. I. Kleinman, F. Brechtel, Y.-N. Lee, L. J. Nunnermacker, and J. Wang (2005), Chemical evolution of an isolated power plant plume during the TexAQS 2000 study, *Atmos. Environ.*, *39*, 3431–3443.

Takegawa, N., Y. Miyazaki, Y. Kondo, Y. Komazaki, T. Miyakawa, J. L. Jimenez, J. T. Jayne, D. R. Worsnop, J. D. Allan, and R. J. Weber (2005), Characterization of an Aerodyne aerosol mass spectrometer (AMS): Intercomparison with other aerosol instruments, *Aerosol Sci. Technol.*, *39*, 760–770, doi:10.1080/02786820500243404.

Takegawa, N., et al. (2006), Evolution of submicron organic aerosol in polluted air exported from Tokyo, *Geophys. Res. Lett.*, *33*, L15814, doi:10.1029/2006GL025815.

Turpin, B. J., and J. J. Huntzicker (1995), Identification of secondary organic aerosol episodes and quantification of primary and secondary organic aerosol concentrations during SCAQS, *Atmos. Environ.*, *29*, 3527–3544.

Turpin, B. J., and H.-J. Lim (2001), Species contributions to PM2.5 mass concentrations: Revisiting common assumptions for estimating organic mass, *Aerosol Sci. Technol.*, *35*, 602–610.

Volkamer, R., J. L. Jimenez, F. San Martini, K. Dzepina, Q. Zhang, D. Salcedo, L. T. Molina, D. R. Worsnop, and M. J. Molina (2006), Secondary organic aerosol formation from anthropogenic air pollution: Rapid and higher than expected, *Geophys. Res. Lett.*, *33*, L17811, doi:10.1029/2006GL026899.

Volz, A., and D. Kley (1985), A resonance-fluorescence instrument for the in-situ measurement of atmospheric carbon monoxide, *J. Atmos. Chem.*, *2*, 345–357.

Weimer, S., F. Drewnick, O. Hogrefe, J. J. Schwab, K. Rhoads, D. Orsini, M. Canagaratna, D. R. Worsnop, and K. L. Demerjian (2006), Size-selective nonrefractory ambient aerosol measurements during the Particulate Matter Technology Assessment Characterization Study—New York 2004 winter intensive in New York City, *J. Geophys. Res.*, *111*, D18305, doi:10.1029/2006JD007215.

Zaveri, R. A., C. M. Berkowitz, J. M. Hubbe, S. R. Springston, F. J. Brechtel, T. B. Onasch, and J. T. Jayne (2004), Nighttime Lagrangian measurements of aerosols and oxidants in the Boston urban plume: Possible evidence of heterogeneous loss of ozone, Proceedings of the 23rd Annual American Association for Aerosol Research Conference, Atlanta, GA, October.

Zhang, Q., M. R. Alfarra, D. R. Worsnop, J. D. Allan, H. Coe, M. R. Canagaratna, and J. L. Jimenez (2005a), Deconvolution and quantification of hydrocarbon-like and oxygenated organic aerosols based on aerosol mass spectrometry, *Environ. Sci. Technol.*, *39*, 4938–4952.

Zhang, Q., D. R. Worsnop, M. R. Canagaratna, and J. L. Jimenez (2005b), Hydrocarbon-like and oxygenated organic aerosols in Pittsburgh: Insights into sources and processes of organic aerosols, *Atmos. Chem. Phys.*, *5*, 3289–3311.

Zhang, Q., M. R. Canagrantna, J. T. Jayne, D. R. Worsnop, and J.-L. Jimenez (2005c), Time- and size-resolved chemical composition of submicron particles in Pittsburgh: Implications for aerosol sources and processes, *J. Geophys. Res.*, *110*, D07S09, doi:10.1029/2004JD004649.

C. Berkowitz, J. Hubbe, and R. A. Zaveri, Atmospheric Science Department, Pacific Northwest National Laboratory, Richland, WA 99352, USA.

F. J. Brechtel, Brechtel Manufacturing Inc., Hayward, CA 94544, USA.

P. H. Daum, L. I. Kleinman, Y.-N. Lee, G. I. Senum, S. R Springston, and J. Wang, Atmospheric Sciences Division, Brookhaven National Laboratory, Bldg 815E, Upton, NY 11973, USA. (kleinman@bnl.gov)

J. Jayne, T. B. Onasch, and D. Worsnop, Aerodyne Research Inc., Billerica, MA 01821, USA.